

Article

The Investigation of Local Scour around Bridge Piers with the Protection of a Quasi-Stumps Group

Yisheng Zhang ^{1,2} , Jiangfei Wang ³, Qi Zhou ³, Yingchun Cai ^{1,2}  and Wei Tang ^{1,2,*}

¹ School of Water Conservancy and Transportation, Zhengzhou University, Zhengzhou 450001, China; yishengzhang@zzu.edu.cn (Y.Z.); yccai@zzu.edu.cn (Y.C.)

² Yellow River Laboratory, Zhengzhou University, Zhengzhou 450001, China

³ Henan Puze Expressway Co., Ltd., Zhengzhou 450046, China; tqycfv@ksdud.com (J.W.); egawxd@ksdud.com (Q.Z.)

* Correspondence: tangwei251231@163.com; Tel.: +86-0371-6778-3172

Abstract: In this study, a quasi-stumps group structure was proposed and placed upstream of the bridge piers to mitigate the scour of the waterflow on the riverbed. Both experiment and numerical simulations using FLOW 3D were employed to study the protective effect of this structure. The numerical results were in good agreement with the experimental findings. It was found that the quasi-stumps group can effectively reduce the flow velocities around the bridge piers, thereby promoting the deposition of suspended sediment. As a result, there was no erosion around the piers, and instead, siltation was formed, which contributed to the stability of the piers. The deposition height around the piers increased as the L (the horizontal distance between the quasi-stumps group and the piers) decreased and both the P (the height of the quasi-stumps group) and S (the ratio of the area of a single leaf on the quasi-stumps group to the cross-sectional area of a single pier) increased. As the L , P , and S increased, the quantity of suspended sediment deposition over the entire riverbed increased. The optimal combination of the quasi-stumps group's protective effect was determined to be $L = D$ (pier diameter), $P = H$ (water depth), and $S = 0.148$.

Keywords: bridge piers; local scour; quasi-stumps group; numerical simulation; FLOW 3D



Citation: Zhang, Y.; Wang, J.; Zhou, Q.; Cai, Y.; Tang, W. The Investigation of Local Scour around Bridge Piers with the Protection of a Quasi-Stumps Group. *Water* **2023**, *15*, 2858. <https://doi.org/10.3390/w15152858>

Academic Editors:
Konstantinos Kaffas, Mike Spiliotis,
Vlassios Hrisanthou
and Helena M. Ramos

Received: 4 May 2023
Revised: 8 July 2023
Accepted: 4 August 2023
Published: 7 August 2023



Copyright: © 2023 by the authors. Licensee MDPI, Basel, Switzerland. This article is an open access article distributed under the terms and conditions of the Creative Commons Attribution (CC BY) license (<https://creativecommons.org/licenses/by/4.0/>).

1. Introduction

The transportation system serves as the cornerstone of national development, and bridges are an integral component of this system. As society progresses, there has been a significant increase in demand for travel and cargo transportation, leading to higher requirements for bridge quantities and capacities. Bridges spanning rivers are particularly crucial, as they not only endure the air corrosion on piers but also the destructive impact of waterflow on pier foundations. Of the two, the latter poses a more significant threat, making river-crossing bridges more susceptible to damage. When water flows through bridge piers, the velocity increases, and the turbulence is intensified near the piers, resulting in backwater upstream of the piers. This creates a pressure gradient from top to bottom, which generates a downward flow that impacts the riverbed. At the same time, the flow on both sides of the piers separates significantly, forming a strong vortex system and a horseshoe vortex with the downward flow. The intense horseshoe vortex generates significant shear stress on the riverbed, causing severe scouring around the bridge piers, resulting in local scour holes. This phenomenon is almost inevitable in alluvial riverbeds, and it affects the stability and safety of bridge piers. Therefore, appropriate measures must be taken during the design stage to prevent scouring. Suitable protective measures can significantly reduce local scouring around bridge piers and improve the safety of bridge structures.

Smith [1] counted and analyzed the causes of 143 bridges that had major accidents from 1847 to 1975 and found that the damage to 70 bridges was caused by the displacement of piers during flooding. The investigation report by Lagasse et al. [2] showed that about

60% of bridge accidents were caused by scours. The scours on riverbeds around piers can also pose threats to people's lives. For example, in April 1987, pier NO. 3 of the bridge crossing the Schoharie River near Fort Hunter, New York, was damaged due to excessive local scour caused by a major flood, resulting in the collapse of the bridge's main girder and the death of 10 people in the accident. In 1989, a bridge on Highway 51 in Tennessee collapsed, and eight people fell into the water and died due to excessive local scour. Although local scours around bridge piers occur all the time, they are particularly strong during floods. During a flood in 1956, the maximum scour depth around pier NO. 7 of the Zhengzhou Yellow River Bridge reached 8 m, and the maximum scour depth around pier NO. 11 reached 14 m, with obvious tilting of the piers. Ultimately, the bridge was destroyed during the catastrophic flood of the Yellow River in 1958. The investigation of the US Federal Highway Administration showed that local scours are one of the primary issues to be considered in bridge design and protection [3]. Therefore, in the process of designing bridge foundations, it is necessary to take some measures to protect the riverbed around the piers, so as to ensure the safety and stability of the piers.

Based on the protective mechanism of a scour, Chiew [4] classified the protective measures of pier foundations into the following two categories: (1) reducing the scouring capacity of a submerged flow and horseshoe vortex in the incoming flow and (2) enhancing the scour resistance of the riverbed materials around bridge piers. Wang et al. [5] referred to these two types of protective measures as active protection and passive protection. Active protective measures include changing the pier shape, collar, slot, sacrificial pile in front of the pier, threaded pier, a splitter plate downstream pier, etc. Jalal and Hassan [6] used FLOW 3D software to study the influence of different pier shapes (circular, rectangular, octagonal, oval, and lenticular) on local scours. The results showed that the scour depth of the lenticular pier was the minimum, while that of the rectangular pier was the maximum. The scour depth of lenticular piers is 40% lower than that of other piers, on average. Jahangirzadeh et al. [7] investigated the effect of different sizes and shapes of collars on reducing the local scour depths around bridge piers. The study found that a collar size $W = 3.0D \sim 3.5D$ can best and most economically reduce the scour depth, where W is the side length of a square collar or the diameter of a circular collar, and D is the pier diameter. Additionally, the square collar provided better protective effects than the circular collar. Nazari-Sharabian et al. [8] used FLOW 3D software to simulate the anti-scouring effect of sacrificial piles with different numbers and different distribution patterns. It was found that, when a single pile is installed in front of a pier, installing a single pile at a distance of five times the pier diameter upstream of the pier can more effectively reduce the scour depth. When three and five piles are installed, the optimal distance for the three piles is six and four times of the pier diameter, and the optimal distance for the five piles is four, six, and eight times the pier diameter. Dey et al. [9] spirally wrapped helical wires and cables on a pier to form a threaded pile. Through experimental studies, it was found that, when the thread angle was 15° and the diameter ratio of the cable to pier was 0.1, the maximum scour depth of the triple-threaded pile could be reduced by 46.3%. The threaded pile could weaken the vortex shedding, which was instrumental in inducing a scour. Furthermore, many researchers have studied the protective effects of active protective measures against scouring a riverbed [10–12]. Passive protection measures include riprap countermeasures, foundation expansion, a tetrahedron frame group, etc. Chiew [13] studied the stability of riprap around piers and identified three different failure modes of riprap: shear failure; settlement failure, and edge failure; a semi-empirical method was proposed to determine the size of the rocks to protect the riprap pile. The experimental data showed that, in the absence of a filter layer, a thicker riprap layer could prevent settlement, and two empirical relationships were proposed for the influence of riprap layer thickness and coverage on the stability of the riprap layer. Parola et al. [14] found that the best protective effect was achieved when the top surface of the expanded foundation was level with the riverbed surface. As the top surface of the foundation lowered or raised, the protective effect weakened accordingly. Li et al. [15] found that the tetrahedron frame group could reduce

the flow velocities around it and dissipate the energy of the waterflow, thus achieving the effect of preventing erosion and promoting sediment deposition, as well as protecting the bedload and suppressing the local scour. In addition, many researchers have studied the passive protective measures [16–18]. The above are the protective measures for the local scour of bridge piers that have been studied more at present.

The above measures are effective in preventing scouring of the riverbed when the flow is clear, but when the water carries silt, these measures cannot effectively cause the suspended sediment in the water to deposit. Therefore, in the case of muddy water, it is necessary to reduce the erosion of the riverbed and also try to make the suspended sediment settle near the bridge piers to fill in the scour holes. At present, most studies on the local scour of piers focus on clean water, while only a few scholars have studied the influence of muddy water on the local scour of piers. For a clear water scour, the sediment is removed from the scour hole but not supplemented by the approach flow. The maximum scouring depth is gradually approached when the flow is no longer capable of removing the bed sediment from the hole. However, for a muddy water scour, the scour hole is continuously provided with sediment by the approach flow. The maximum scouring depth is reached when the average amount of sediment transported into the scour hole by the approach flow is equal to the average amount of sediment removed from the hole due to the local scour. Therefore, the maximum scouring depth fluctuates periodically about a mean value [19].

For erosion in muddy water, the current methods to reduce the scour depth include installing plants and thin cylinders, etc. upstream of piers, and the main research methods are experiments and numerical simulations. Abt et al. [20] studied the sediment deposition and retention capacity in vegetated riverbeds. The results showed that the presence of vegetation not only promotes the deposition of suspended sediment but also causes some suspended sediment to adhere to the vegetation. Ultimately, vegetation can retain 30~70% of suspended sediment, and it was found that the amount of sediment siltation is mainly related to the flow and the length of the plant leaves. Sun et al. [21] studied the effect of tall and short submerged plants on suspended sediment deposition in a turbid water tank. It was found that the siltation was seven times greater when tall and short plants were mixed than when no plants were present, the effect of promoting sediment deposition was the next most effective when only tall plants were present, and the effect gradually increased with the decrease in plant spacing. Nabaei et al. [22] studied the influence of vegetation on the flow structure and turbulence anisotropy around a semi-elliptical abutment. They found that the presence of vegetation in the channel significantly reduced the primary vortex. The tangential and radial velocities decreased with the vegetation in the channel bed, and the Reynolds shear stress in the channel decreased obviously. Amir et al. [23] studied the impact of vegetation coverage on local scours around bridge piers. The results indicated that the depth of the local scour around bridge piers in a water tank with vegetation was only half of that without vegetation, and the scour equilibrium time was reduced by 42% compared to that without vegetation. Wang et al. [24] studied the influence of the arrangement density, water depth, and sediment particle size on the sediment starting velocity by installing flexible rubber cylinders parallel in a water tank. The experimental results showed that the starting velocity of the sediment increased with the decrease in the arrangement density and the increase in the water depth and sediment particle size, and the corresponding equation of the starting velocity of the sediment was derived. Tang et al. [25] set up stainless steel fine cylinders with different arrangement densities and diameters in still water and measured the sediment settling velocities of particles with diameters ranging from 0.1 cm to 0.45 cm. The study found that, within the experimental particle size range, the settling velocity of the sediment in the presence of slender cylinders decreased with the increase of the cylinder density and sediment particle size. They also derived a sediment settling velocity formula that took into account the density and diameter of the slender cylinders. Zhao et al. [26] investigated the influence of the submerged vegetation density λ on the turbulent flow characteristics of an open channel.

The results showed that, for $0.04 < \lambda < 0.1$, the turbulent statistical profiles exhibited similar characteristics to the bed shear flow and free shear flow. When $\lambda = 1.44$, the turbulent statistics above the vegetation top exhibited features of a boundary shear flow. Xiong et al. [27] proposed and verified a three-dimensional simulation model for a live bed pier scour considering suspended sediment loads, which could simulate the dynamic balance of inputs and outputs of sediment around the piers in a reliable and computationally efficient manner. Yu et al. [28] employed six different RANS turbulence models to simulate the flow structure in an open channel with a developed vegetation patch and compared the results with the experimental data. They concluded that CFD is an effective research method and also observed that different turbulence models exhibited varying simulation performances. Chen et al. [29] used FLOW 3D software to conduct numerical simulations of the hydraulic characteristics of rigid submerged plants. They modified the Shields number from the perspective of turbulent kinetic energy and improved the sediment module, so that the FLOW 3D software could simulate the flow field and sediment movement more accurately, and the results of the numerical simulation were in good agreement with the experimental data. Compared with a single pier, a group of piers are increasingly used in bridge constructions. A group of piers is shown in Figure 1. Therefore, many scholars have studied the local scours around groups of piers in riverbeds through experiments and numerical simulations. They have found that the waterflow between groups of piers is obviously discontinuous and nonlinear, and the scouring process in riverbeds has also become more complex [30–34]. Studying the sediment movement around groups of piers in rivers has more reference value for practical engineering.



Figure 1. A group of bridge piers.

Based on the above content, a quasi-stumps group structure placed upstream of bridge piers was proposed in this study. This structure can effectively lower the flow velocities around bridge piers, impede the transportation of bedload sediment, and intercept suspended sediment, so as to achieve the purpose of reducing the local scour. Additionally, it can provide protection against floating objects upstream colliding with bridge piers. The group of piers used in this study was obtained by proportionally reducing the actual engineering and consisted of six circular piers. In this paper, the protective effect of the quasi-stumps group on the riverbed around the bridge piers was studied by experiment and numerical simulations. The effects of three factors (the distance between the quasi-stumps group and the bridge pier, the height of the quasi-stumps group, and the leaves area of the quasi-stumps group) of this structure on the protective effect were also analyzed. Based on the analysis results, the combination of a quasi-stumps group with the best protective effect was proposed.

2. Materials and Methods

2.1. Structure of Quasi-Stumps Group

The quasi-stumps group structure placed upstream of the piers was proposed to reduce the local scour in the riverbed around the piers. The quasi-stumps group is composed of nine quasi-stumps. A single quasi-stump of 8 cm high (one-third the water depth)

contains twelve leaves. The top view and side view of the quasi-stumps group are shown in Figure 2 (D is the pier diameter). The structure not only reduces the flow velocities reaching the piers, thus reducing the erosion of the riverbed by the flow, but also promotes the suspended sediment in the water to be deposited around the piers to replenish the scour holes.

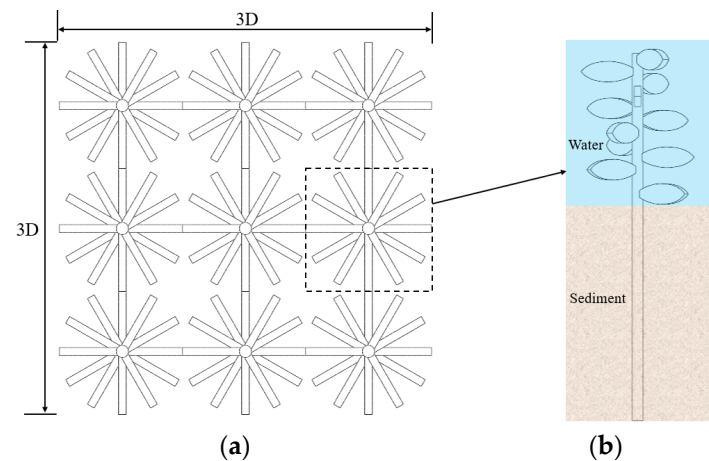


Figure 2. The structure of the quasi-stumps group. (a) Top view. (b) Side view.

2.2. Experimental Setup

The experiments were carried out in the hydraulic laboratory at Zhengzhou University's School of Water Conservancy and Civil Engineering. The experimental platform consists of a rectangular channel made of glass with dimensions of 72 cm (width) \times 50 cm (height) and a length of 12 m, two water tanks, a pumping station, a circulating pipe, an electromagnetic flowmeter, a valve, a sand mixing pool, the group of bridge piers, and the quasi-stumps group installed in the sink, as shown in Figure 3. In order to achieve flow stability, a channel measuring 4.3 m in length was positioned at the forefront of the group of piers. The water in the experiment was a silt-carrying flow with a sediment content of 2.7 kg/m³, meaning that each cubic meter of water and sand mixture contained 2.7 kg of sediment. The median grain size of the sediment in the inlet flow was 0.063 mm. In the experiment, the median grain size (d_{50}) of the sediment in the riverbed was 0.34 mm, and the sediment particle size ranged from 0.15 mm to 0.41 mm in diameter. The median grain size of the sediment in the riverbed used in this study was referenced from the experiments of Jahangirzadeh et al. [35] and Obied et al. [36]. The median particle size and sediment content of the suspended sediment in the inlet flow were from the study of Debnath and Chaudhuri [37]. The thickness of the sediment was 10 cm (in the preliminary experiment, the scour depth of the riverbed was much smaller than 10 cm). The density of the sediment was 2650 kg/m³. The underwater angles of repose for the sediment in the riverbed and inlet flow were 32° and 30°, respectively. Each experiment lasted for the duration of one hour, which matched the duration of the numerical simulation. Prior to each experiment, the flume was gradually filled with water to ensure saturation of the riverbed material. Measurements of the water depth, scour depth, deposit depth, and velocities were taken using a needle water level gauge and a flow velocity meter, respectively. To minimize the wall effects on the scour rate, the flume width was maintained at a minimum of 10 times the diameter of the pier [38], which was set to 6 cm based on the dimensions of the experimental flume.

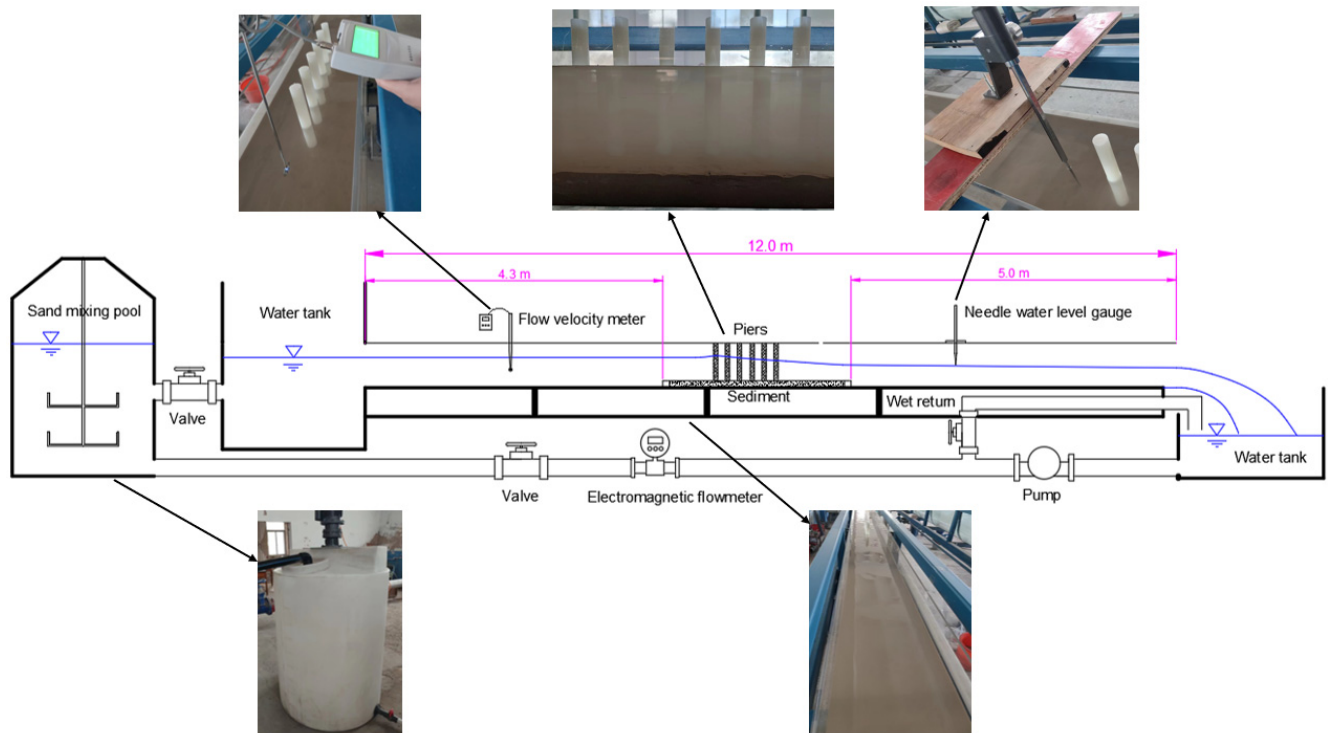


Figure 3. The experimental facilities.

The group of piers in the experiment consists of six piers, and the piers are numbered as shown in Figure 4. The model of the group of piers is obtained by proportionally reducing the piers of the Yellow River Super Major Bridge of Yangxin Expressway from Puyang City to Hubei Province, and the scale is 100:3. In the experiment, the flow velocity upstream of the piers is controlled at 0.48 m/s, which is obtained by converting the flow velocity in the actual project to the model experiment. The scale of the flow velocity is $\sqrt{100/3}$.

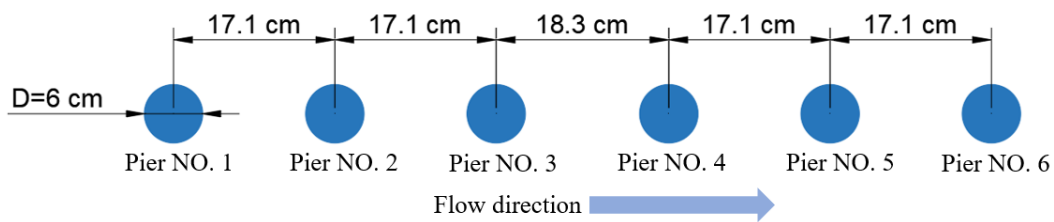


Figure 4. The dimensions, spacing, and numbers of the piers group.

2.3. Numerical Simulation

FLOW 3D uses the RNG $k-\epsilon$ turbulence model to solve Reynolds-averaged Navier–Stokes equations. It is an improved version of the $k-\epsilon$ turbulence model, where RNG stands for “renormalization group”. It is a method that utilizes the theory of a renormalization group from statistical physics to model turbulence. k is the turbulent kinetic energy, and it refers to the intensity or energy of the vortical motion in a turbulent flow field. In turbulence, the fluid contains vortices of various scales that continuously interact and exchange energy. Turbulent kinetic energy quantifies the strength of these vortices and is described in the turbulent model by an equation governing its evolution. ϵ is the turbulent dissipation rate, and it represents the rate at which turbulent kinetic energy is transformed or dissipated. Turbulence is a process of continuous energy conversion, where kinetic energy is converted into internal energy, and there is also a process of internal energy returning to kinetic energy. The turbulent dissipation rate describes the rate of this energy conversion or dissipation and is described in the model by an equation governing its evolution.

The hydrodynamics solver employed in this study is fully coupled with the sediment transport module, enabling the combined use of semi-empirical formulas and hydraulic principles to predict the riverbed evolution. The equilibrium states of the scour are determined by analyzing changes in the riverbed and calculating the flow field.

The turbulent flow in this study is governed by the continuity equation, which can be mathematically expressed as follows:

$$V_F \frac{\partial \rho}{\partial t} + \frac{\partial}{\partial x}(\rho u A_x) + R \frac{\partial}{\partial y}(\rho v A_y) + \frac{\partial}{\partial z}(\rho w A_z) + \zeta \frac{\rho u A_x}{x} = R_{DIF} + R_{SOR} \quad (1)$$

where V_F is the fractional volume open to flow; ρ is the fluid density; (u , v , and w) are the velocity components in the (x , y , and z) directions, respectively; (A_x , A_y , and A_z) are the portion of area open to flow in the (x , y , and z) directions, respectively; R_{DIF} is the turbulent diffusion term; R_{SOR} is the mass source; R is a coefficient that depends on the chosen coordinate system; and ζ is related to the compressibility of the fluid. In this numerical simulation, water is an incompressible fluid, and the Cartesian coordinate system is used, so $R = 1$ and $\zeta = 0$. x is the coordinate value along the x -axis.

The equations of motion for the fluid velocity components (u , v , and w) in the three coordinate directions are Navier–Stokes equations with some additional terms:

$$\frac{\partial u}{\partial t} + \frac{1}{V_F} \left(u A_x \frac{\partial u}{\partial x} + v A_y \frac{\partial u}{\partial y} + w A_z \frac{\partial u}{\partial z} \right) = -\frac{1}{\rho} \frac{\partial p}{\partial x} + G_x + f_x - b_x - \frac{R_{SOR}}{\rho V_F} (u - u_w - \delta u_s) \quad (2)$$

$$\frac{\partial v}{\partial t} + \frac{1}{V_F} \left(u A_x \frac{\partial v}{\partial x} + v A_y \frac{\partial v}{\partial y} + w A_z \frac{\partial v}{\partial z} \right) = -\frac{1}{\rho} \frac{\partial p}{\partial y} + G_y + f_y - b_y - \frac{R_{SOR}}{\rho V_F} (v - v_w - \delta v_s) \quad (3)$$

$$\frac{\partial w}{\partial t} + \frac{1}{V_F} \left(u A_x \frac{\partial w}{\partial x} + v A_y \frac{\partial w}{\partial y} + w A_z \frac{\partial w}{\partial z} \right) = -\frac{1}{\rho} \frac{\partial p}{\partial z} + G_z + f_z - b_z - \frac{R_{SOR}}{\rho V_F} (w - w_w - \delta w_s) \quad (4)$$

where (G_x , G_y , and G_z) are the body accelerations in the (x , y , and z) directions; (b_x , b_y , and b_z) are the flow losses through porous media in the (x , y , and z) directions; and (f_x , f_y , and f_z) are the viscous accelerations in the (x , y , and z) directions, respectively. Viscous acceleration describes the acceleration experienced by a moving object in fluid due to the influence of viscous forces. When an object moving in fluid changes its velocity or direction, the surrounding fluid's viscous forces cause the object to undergo an additional acceleration exerted by the fluid, and this acceleration is known as the viscous acceleration. (u_w , v_w , and w_w) are the speeds of the source components, they are used in simulations to represent the velocities of the source component of an external input or perturbation. The velocities can be used to simulate injection, withdrawal, agitation, or other external influences in the fluid. t is the time, and p is the pressure. The determination of the δ value is related to the type of the source. When the source is the stagnation pressure type, $\delta = 0$. When the source is the static pressure type, $\delta = 1$. $\delta = 1$ in this study. (u_s , v_s , and w_s) are the velocities of the fluid relative to the source at its surface, and they represent the relative relationships between the velocities of the fluid on the surface of the source and the movements of the source itself. In FLOW 3D, to accurately simulate sediment erosion, it is necessary to consider the relative motion of the flow and sediment particles, as well as their shape and velocity distribution, in order to better simulate the interaction between the flow and sediment. In this numerical simulation, the sources are the waterflow and the sediment in the inlet flow.

The properties of various non-cohesive sediments can be set in the sediment scour model, including the grain size, mass density, angle of repose, critical shear stress, and parameters for entrainment and transport. In FLOW 3D, sediment has two states of existence: suspended and packed sediment. The sediment movement is estimated through the prediction of the sediment erosion, advection, and deposition processes.

Due to the impracticality of computing the flow dynamics for individual sediment grains, an empirical model is employed. In FLOW 3D, the model utilized is based on the work of Mastbergen and van den Berg [39]. The critical Shields parameter is calculated

using the Soulsby–Whitehouse equation [40]. The first step in calculating the critical Shields parameters is to compute the dimensionless parameters $d_{*,i}$:

$$d_{*,i} = d_i \left[\frac{\rho_f (\rho_i - \rho_f) \|\mathbf{g}\|}{\mu_f^2} \right]^{1/3} \tag{5}$$

where i represents the i th type of sediment, as multiple sediments with different characteristics can be defined in FLOW 3D; d_i is the sediment diameter; ρ_f is the fluid density; ρ_i is the sediment density; $\|\mathbf{g}\|$ is the magnitude of the acceleration of gravity \mathbf{g} ; and μ_f is the dynamic viscosity of the fluid. The dimensionless critical Shields parameter $\theta_{cr,i}$ is computed using the Soulsby–Whitehouse equation [40]:

$$\theta_{cr,i} = \frac{0.3}{1 + 1.2d_{*,i}} + 0.055[1 - \exp(-0.02d_{*,i})] \tag{6}$$

The modification is applied to the dimensionless critical Shields parameter of sediment on the slope $\theta'_{cr,i}$ [40]:

$$\theta'_{cr,i} = \theta_{cr,i} \frac{\cos\alpha \sin\beta + \sqrt{\cos^2\beta \tan^2\varphi - \sin^2\alpha \sin^2\beta}}{\tan\varphi} \tag{7}$$

where α represents the angle between the upslope direction and flow direction, while β denotes the angle of the bed slope, and φ indicates the user-defined angle of repose of the sediment.

The calculation of the local Shields parameter θ_i is as follows:

$$\theta_i = \frac{\tau}{\|\mathbf{g}\| d_i (\rho_i - \rho_f)} \tag{8}$$

where τ is local bed shear stress.

The calculation for the entrainment lift velocity $\mathbf{u}_{lift,i}$ is as follows [39]:

$$\mathbf{u}_{lift,i} = \alpha_i \mathbf{n}_s d_{*,i}^{0.3} (\theta_i - \theta'_{cr,i})^{1.5} \sqrt{\frac{\|\mathbf{g}\| d_i (\rho_i - \rho_f)}{\rho_f}} \tag{9}$$

where α_i represents the entrainment parameter, while \mathbf{n}_s denotes the outward-pointing normal line at the packed bed interface.

The equation proposed by Soulsby [40] to calculate the settling velocity of sediment $u_{settling,i}$ is used:

$$u_{settling,i} = \frac{v_f}{d_i} \left[\left(10.36^2 + 1.049d_{*,i}^3 \right)^{0.5} - 10.36 \right] \tag{10}$$

where v_f is the kinematic viscosity of fluids. The assumption is made that the settling motion occurs aligned with the force of gravity:

$$\mathbf{u}_{settling,i} = u_{settling,i} \frac{\mathbf{g}}{\|\mathbf{g}\|} \tag{11}$$

To describe the interactions between particles, the settling velocity is determined using the Richardson-Zaki correlation:

$$\mathbf{u}_{settling}^* = \mathbf{u}_{settling,i} [1 - \min(0.5, c_s)]^{\zeta} \tag{12}$$

where c_s represents the volumetric fraction that accounts for the total amount of suspended sediment. ζ is computed as

$$\zeta = \zeta_{user} \zeta_0 \quad (13)$$

where ζ_{user} is the Richardson-Zaki coefficient multiplier, and ζ_0 represents the Richardson-Zaki coefficient.

By utilizing Equation (14), the dimensionless bedload transport rate Φ_i [41] was determined, while Equation (15) was employed to calculate the volumetric bedload transport rate $q_{b,i}$:

$$\Phi_i = \beta_i (\theta_i - \theta'_{cr,i})^{1.5} C_{b,i} \quad (14)$$

$$q_{b,i} = \Phi_i \left[\|\mathbf{g}\| \left(\frac{\rho_i - \rho_f}{\rho_f} \right) d_i^3 \right]^{1/2} \quad (15)$$

where the coefficient β_i typically equals 8.0, while $C_{b,i}$ represents the volume fraction of the sediment.

2.4. Computational Domain

Based on the experimental conditions, the dimensions of the simulation region were 270 cm in length, 72 cm in width (12D), and 44 cm in height. The distance between pier NO. 1 and the inlet was 76 cm (12.6D), and the distance between pier NO. 6 and the outlet was 108 cm (18D). The initial riverbed had a sediment thickness of 10 cm, while each individual pier had a diameter of 6 cm. The median particle size of the sediment was 0.34 mm. The water depth was 24 cm (4D). Moreover, in order to prevent the initial scouring, baffles with a height matching that of the riverbed were positioned at both the inlet and outlet locations, as shown in Figure 5a. For the boundary conditions, the inlet was specified as a velocity inlet, while the outlet was set as the outflow. The boundaries on both sides were defined as walls. The top mesh was assigned a symmetric boundary condition, and there was an 8 cm high air space between the water surface and the top mesh, as shown in Figure 5b. A structured orthogonal grid was implemented across all the computing domains. The main body utilized a grid size of 0.012 m \times 0.012 m \times 0.012 m, while the grid size in the area of the quasi-stumps group was 0.0036 m \times 0.0036 m \times 0.0036 m. The sediment concentration of the inlet flow was 2.7 kg/m³, and the median particle size of the sediment was 0.063 mm. The sediment in the riverbed had a critical Shields number of 0.061, an entrainment coefficient of 0.018, and a bedload coefficient of 8. Regarding the suspended sediment, its critical Shields number was 0.043, the entrainment coefficient was 0.02, and the bedload coefficient was 9.3. The RNG k- ϵ turbulence model was used in this numerical simulation, and the free surface of the flow was tracked using the Tru VOF method.

The grid is the basis of the numerical simulation. The degree of discretization of the equations is determined by the grid partition, while the accuracy and stability of the calculations depend on the size of the grid partition. Therefore, a sensitivity analysis of the grid size is required, as shown in Table 1. Taking the scouring of the piers group without the quasi-stumps group as an example, d_m is the maximum scouring depth, and d_a is the average scouring depth in Table 1. Ten points are selected in the scour pit, and their scour depths are measured, and the average scour depth is obtained by calculating their average value. The sensitivity analysis shows that, while the grid size decreased to 0.012 m, the mean error tended to be stable and less than 5%; when size decreased to 0.010 m, the mean error only decreased by 0.3%; however the number of grids increased by 364,185, which made the calculation time twice as long as the original one. Therefore, taking into account the error and computational time, a grid size of 0.012 m was determined as the optimal choice for the numerical simulation.

Prior to conducting the actual experiments, the pre-experiment and its corresponding numerical simulations of the scour in the riverbed around the bridge piers without the quasi-stumps group were performed. According to the criterion of Chiew [4], the experiment's

duration was determined based on the point at which the change in the scour depth remained below 1 mm for a continuous period of eight hours, indicating that the scour reached its equilibrium state and maximum depth. In the pre-experiment, it took 62 h to attain scour equilibrium. The scouring area is the sum of the areas where the scour depth exceeds 1 mm. The variation in the maximum scouring depth and scouring area with time are shown in Figure 6. After one hour, the increase in the maximum scouring depth and scouring area became very small. The maximum scour depth and scour area of the simulation reached 97.1% and 96.0% of the maximum value, respectively, and the results of the experiment attained 96.4% and 95.8% of the maximum value, respectively. Therefore, the experimental duration and simulated time were both configured for a period of 3600 s.

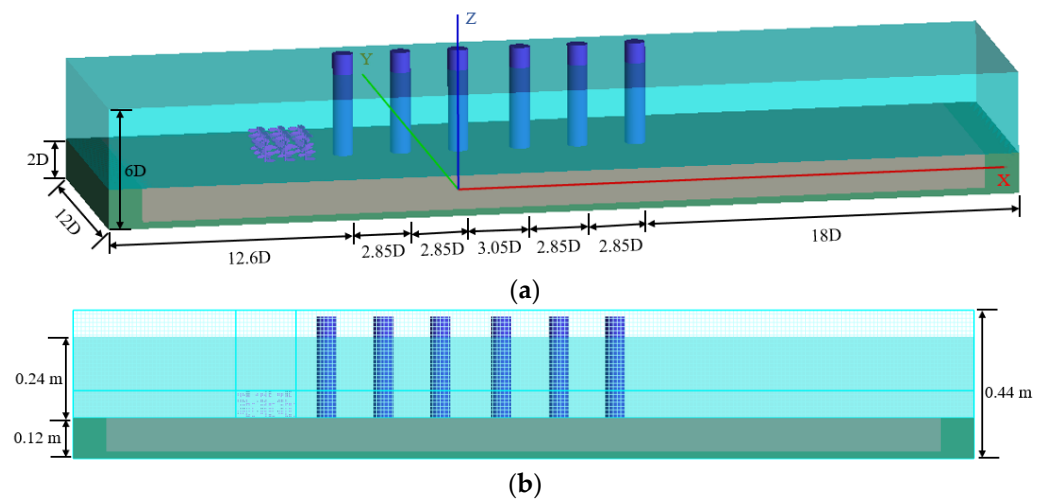


Figure 5. The model of the numerical calculations. (a) Overview and dimensions of the model. (b) Side view of the grids.

Table 1. The sensitivity analysis of the mesh size.

Test Number	Mesh Size (m)	Mesh Number	Numerical Simulation		Laboratory Experiment		Mean Error
			d_m	d_a	d_m	d_a	
1	0.016	216,384	0.0178	0.0153			13.1%
2	0.014	305,133	0.0171	0.0145			7.9%
3	0.012	491,175	0.0166	0.0141	0.0159	0.0134	4.8%
4	0.010	855,360	0.0166	0.0140			4.5%

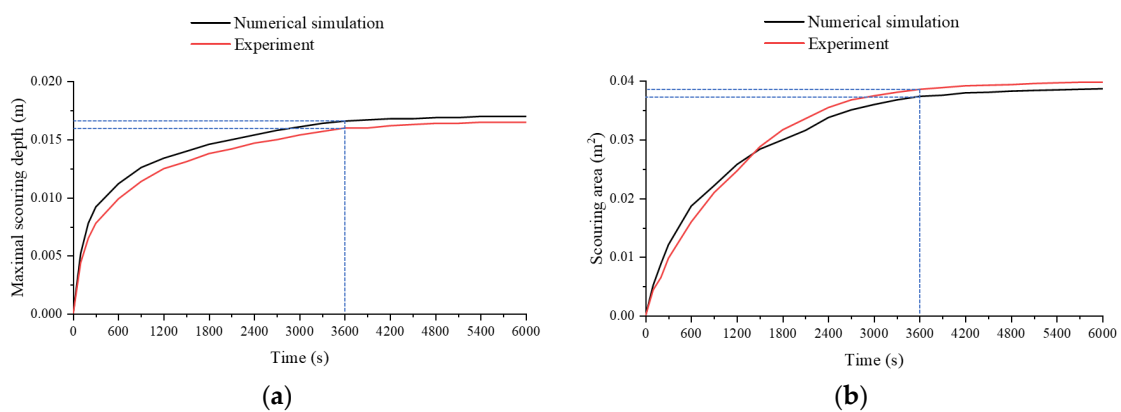


Figure 6. The contrast in the experimental (red) and simulated (black) variations of the maximum scouring depth. (a) and scouring area (b) with time. (a) Maximum scouring depth. (b) Scouring area.

2.5. Experimental Variables and Working Conditions

A total of 12 groups of experiments were set up in this study, among which the experiment NO. 0 did not include the quasi-stumps group. It was used to compare with the experiments involving the quasi-stumps group in order to analyze the protective effect of the quasi-stumps group on the riverbed scour around the bridge piers. In addition, the influence of different quasi-stumps groups on the protective effect was also studied. Three factors were set for the quasi-stumps group: the distance between the quasi-stumps group and bridge piers, the height of the quasi-stumps group, and the area of leaves on the quasi-stump. There were five different values for the distance and leaves area and three different values for the height, which were used to analyze the degree of influence of different factors on the protective effect. The experimental working conditions were set up as shown in Table 2. In Table 2, V is the average flow velocity upstream of pier NO. 1, H is the water depth, S is the ratio of the area of a single leaf to the cross-sectional area of a single pier, P is the height of the stumps group in the water, and L is the horizontal distance between the downstream edge of the stumps group and the upstream edge of pier NO. 1. The meanings of L , P , and S are shown in Figure 7. The meanings of these symbols are added to Appendix A.

Table 2. The experimental working conditions.

Experimental Number	V (m/s)	H (m)	S	P	L
0			Without quasi-stumps group		
1			0.088	$H/3$	D
2			0.088	$H/3$	$2D$
3			0.088	$H/3$	$3D$
4			0.088	$H/3$	$4D$
5	0.48	0.24	0.088	$H/3$	$5D$
6			0.088	$2H/3$	D
7			0.088	H	D
8			0.103	$H/3$	D
9			0.118	$H/3$	D
10			0.133	$H/3$	D
11			0.148	$H/3$	D

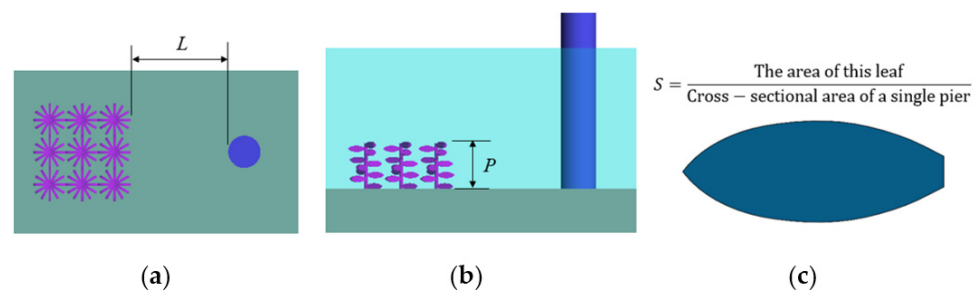


Figure 7. The meanings of L (a), P (b), and S (c).

2.6. Grid and User-Defined Parameters

The mesh is a structured finite-difference mesh featuring rectangular prism-shaped cells, which ensures an efficient computational performance and few cumulative numerical errors. In contrast to the typical body-fitting mesh, the mesh of FLOW 3D is less accurate in describing complex geometric shapes. Therefore, in order to ensure that all structures are

identified, it is necessary to perform local mesh encryption in areas with small geometry dimensions. It is important to maintain a size ratio of no more than 5 between neighboring grids and also that the particle size of the sediment is less than one-tenth of the grid size. It is very important to find a suitable mesh size; if the size is too big, it will not be able to accurately capture the outline of the piers and quasi-stumps group, which will affect the accuracy of the calculations; if it is too small, it will increase the time required for the calculations. Consequently, it is crucial to strike a balance between precision and computational resources when determining an appropriate mesh size. Figure 8 presents the top-down perspective of the computed meshes surrounding the quasi-stumps group and piers. Figure 9 illustrates the outline of the quasi-stumps group and piers captured by the grid. The most suitable grid size for this numerical simulation was found by trying.

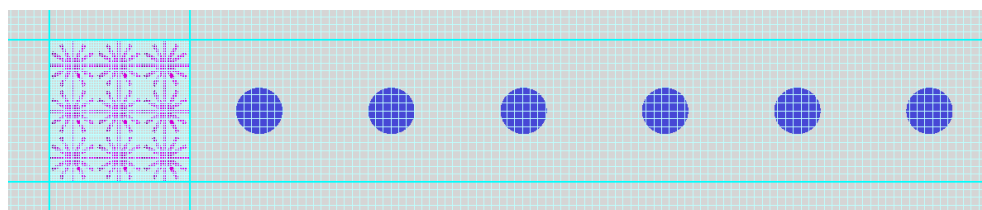


Figure 8. The top-down view of the grids for the quasi-stumps group and piers.

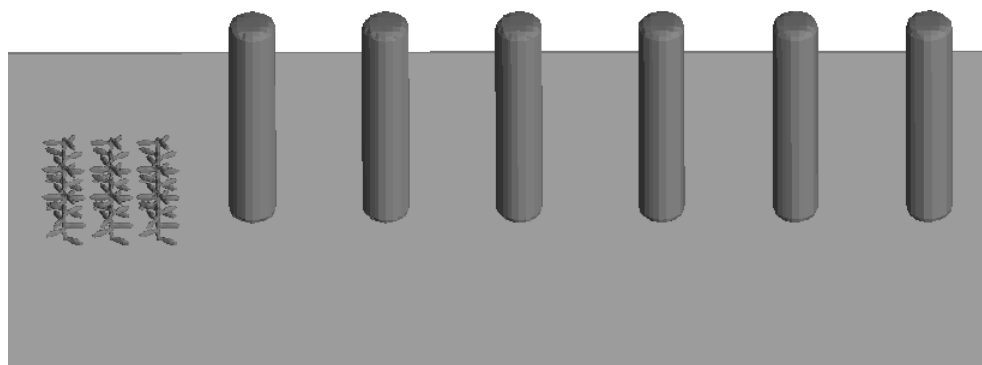


Figure 9. The outline of the quasi-stumps group and piers captured by the grids.

The effect of user-defined parameters on sediment movement was studied before conducting the actual experiment. The user-defined parameters include the underwater angle of repose φ , maximum packing fraction C_V , entrainment coefficient α , and bedload coefficient β . The maximum packing factor C_V of the sediment is the highest density of sediment particles packed on the riverbed. When the maximum packing factor is reached, the gap between sediment particles is the smallest, and the most compact state of accumulation is reached. (1) The underwater angle of repose φ of the sediment in the numerical simulation is the same as that of the sediment used in the experiment. (2) As the maximum packing fraction C_V increases within the range of (0,1), there is a small reduction in the diffusion height of the suspended sediment. It is observed that the maximum scouring depth at $C_V = 0.1$ is only 5.8% higher compared to $C_V = 0.9$. Therefore, the variation of C_V has little influence on the depths of the scour holes. C_V is set to 0.64. (3) The depths of the scour holes are significantly influenced by the entrainment coefficient α . A higher value of α leads to a greater amount of sediment being carried away by the flow, resulting in accelerated erosion of the riverbed. At $\alpha = 0.018$ and $\alpha = 0.4$, the depth of the scour hole is 2.5 and 5.1 times greater, respectively, compared to $\alpha = 0.001$. The α of the bedload sediment and suspended sediment are set to 0.018 and 0.02, respectively. (4) The magnitude of sediment transport along the riverbed increases with an increase in the bedload coefficient β . The scouring depth is 1.5 times higher at $\beta = 13$ compared to

$\beta = 0.058$, indicating that the effect of the β value on the scour depth is small. The β values of the bedload sediment and suspended sediment are set to 8.0 and 9.3, respectively.

3. Results

3.1. Validation

In experiment NO. 3, the experimental and simulated siltation are shown in Figure 10. It is evident that the simulated outcomes are in close agreement with the experimental results. The regions that cause siltation are approximately the same in the experiment and simulation. The relative error between the simulated and experimental results of the maximum siltation height was only 5.7% by measurement.

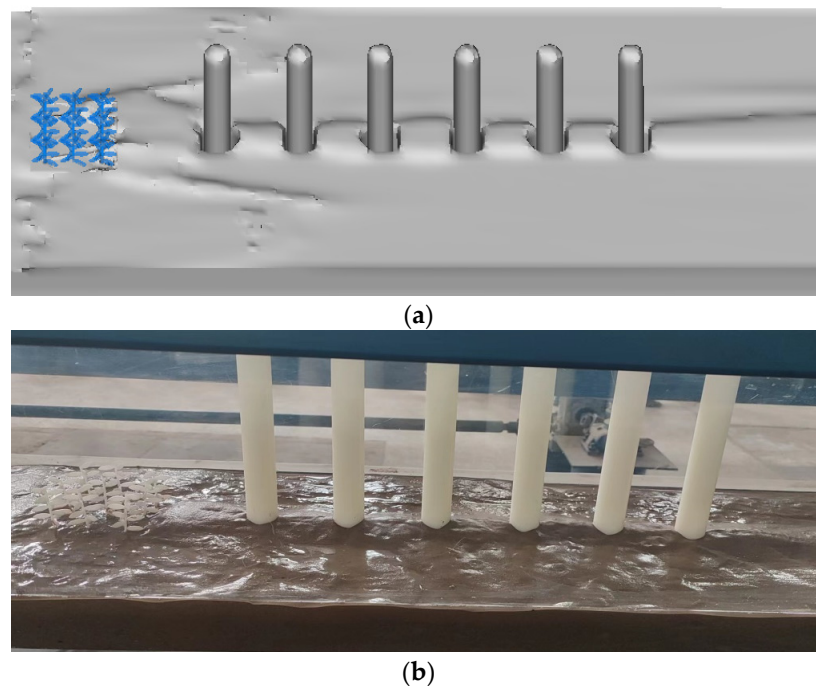


Figure 10. The comparison of the simulated (a) and experimental (b) results of the silted riverbed for experiment NO. 3. (a) The results of the numerical simulation. (b) The results of the experiment.

The flow velocity is the primary factor causing erosion and deposition in riverbeds, so before verifying the three-dimensional topography of the sedimentation, it is necessary to compare the agreement between the experimental and numerical simulation flow fields. Five measurement points were selected around the bridge piers, as shown in Figure 11.

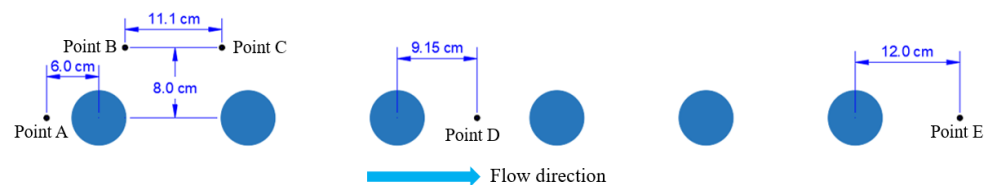


Figure 11. The locations of points A, B, C, D, and E.

Validation was conducted on experiments NO. 0, NO. 5, and NO. 10, with all points located at one-fourth of the water depth. The flow velocities and relative errors for each point in the experiment and numerical simulation are presented in Table 3. The relative error is calculated as follows:

$$\text{Relative error} = \frac{\text{Simulated value} - \text{Experimental value}}{\text{Experimental value}} \times 100\% \quad (16)$$

Table 3. Relative errors between the numerical simulated and experimental flow velocity (m/s) at each point for experiments NO. 0, 5, and 10.

Points	Experiment NO. 0			Experiment NO. 5			Experiment NO. 10		
	Experiment	Numerical Simulation	Relative Error	Experiment	Numerical Simulation	Relative Error	Experiment	Numerical Simulation	Relative Error
Point A	0.341	0.332	−2.64%	0.233	0.253	8.58%	0.044	0.045	2.27%
Point B	0.447	0.423	−5.37%	0.338	0.354	4.73%	0.221	0.219	−0.90%
Point C	0.438	0.411	−6.16%	0.334	0.347	3.89%	0.229	0.225	−1.75%
Point D	0.147	0.144	−2.04%	0.121	0.123	1.65%	0.082	0.085	3.66%
Point E	0.253	0.254	0.40%	0.205	0.206	0.49%	0.147	0.148	0.68%

From Table 3, it can be observed that the relative errors between the numerical simulation and experiment flow velocities ranged from −6.16% to 8.58%, with the highest relative error occurring at point A of experiment NO. 5. This indicates a good agreement between the numerical simulated and experimental flow fields.

The simulated results of the dimensionless maximum deposition height d_h/D and deposition area A_h/A_D are compared with the experimental results to validate the accuracy of the simulated results obtained using FLOW 3D, where d_h is the maximum deposition height, A_h is the deposition area on the riverbed, and A_D represents the cross-sectional area of a single pier: $A_D = \pi D^2/4$. The meanings of these symbols are added to Appendix A. Figure 12 shows a comparison between the experimental and simulated results of d_h/D and A_h/A_D at 60 min. The data in Figure 12 are from experiments NO. 1 to 11. Formula (16) was used to calculate the relative errors. The boundary lines in Figure 12 are the straight lines passing through the origin point and the point of the maximum relative error. The relative error of the dimensionless deposition height (Figure 12a) ranged from −9.44% to 4.87%, respectively, and the dimensionless deposition area (Figure 12b) ranged from −7.76% to 12.33%, respectively. Under various conditions, the simulated results demonstrated a maximum relative error of 12.33% in comparison to the experimental findings, which indicated that the numerical simulation and the experiment were in good agreement. Therefore, FLOW 3D software can be used to study the erosion and sedimentation around bridge piers with a quasi-stumps group.

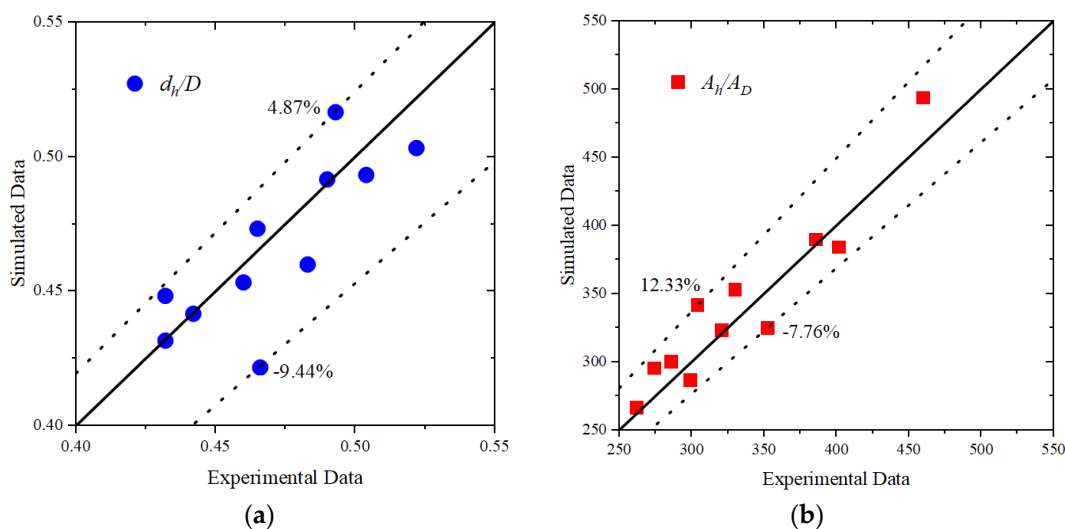


Figure 12. Comparison of the simulated and experimental data for the maximum deposition height (a) and deposition area (b). (a) Maximum deposition height. (b) Deposition area.

Although there is good agreement between the numerical simulated and experimental results regarding the maximum deposition height and deposition area, this does not necessarily imply that the deposition patterns in the numerical simulations and experiments are

identical. Therefore, it is also necessary to compare the location generating the maximum deposition height and the distribution of the deposition areas. By selecting experiments NO. 2, NO. 4, NO. 6, NO. 8, and NO. 10, the locations generating the maximum deposition height in both the experiments and simulations were compared. Their spatial distribution is illustrated in Figure 13a. Through measurements and calculations, it was found that the average distance between the highest deposition points in the experiments and simulations was 6.34 cm (1.06D). This indicates that the positions generating the maximum deposition in the experiments and simulations were relatively close. Experiments NO. 3, NO. 5, and NO. 9 were selected to compare the deposition distributions between the experiments and simulations. The comparison for experiment NO. 9 is illustrated in Figure 13b. Through measurements and calculations, it was found that the overlapping deposition area accounted for 82.25% of the total experimental area on average. Therefore, the distribution of deposition areas in the simulations closely approximated that of the experiments.

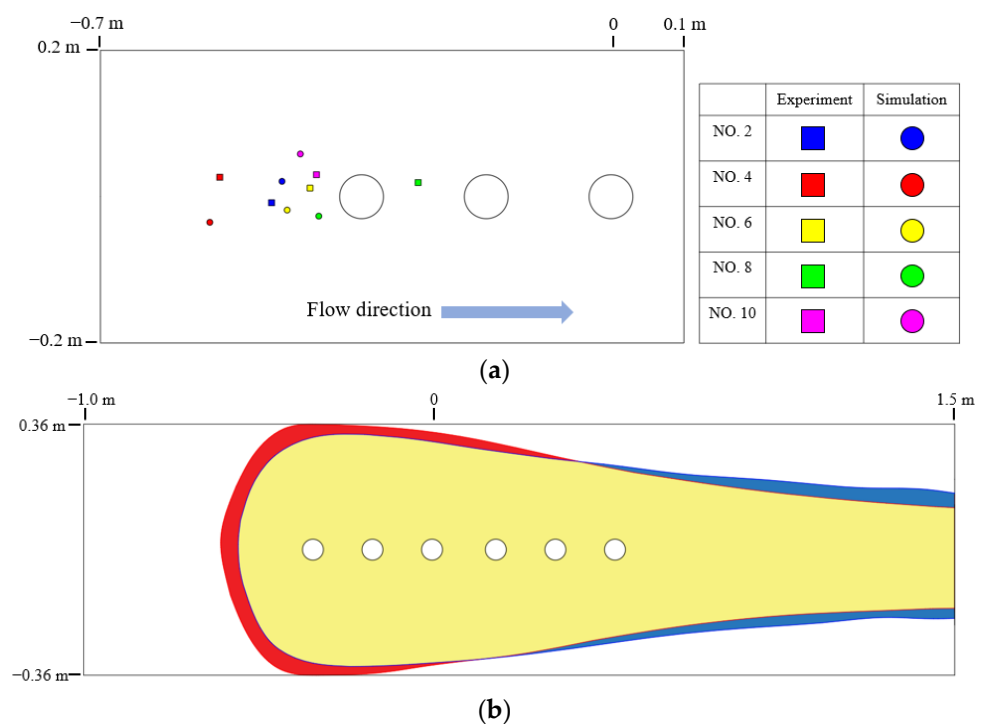


Figure 13. A comparison between the locations generating the maximum deposition height (a) and the distribution of the deposition areas (b) in the experiments and simulations. (a) The locations generating the maximum deposition height in the experiments and numerical simulations. (b) The distribution of the deposition areas in the numerical simulation and experiment for experiment NO. 9. The first column of the table indicates the number of the experiment, for example, NO. 2 represents experiment No. 2. Yellow represents the overlapping deposition areas between the simulation and experiment, red represents the deposition areas unique to the numerical simulation, and blue represents the deposition areas unique to the experiment.

3.2. Protective Effect of the Quasi-Stumps Group

The three-dimensional riverbed topography after being scoured and silted at 3600 s without (experiment NO. 0) and with (experiment NO. 3) the quasi-stumps group is shown in Figure 14. In the absence of the quasi-stumps group, the riverbed around piers NO. 1 and NO. 2 was seriously scoured, which threatened the stability of the piers. In the presence of the quasi-stumps group, the riverbed around the piers was not scoured; instead, a large amount of sediment was deposited upstream of pier NO. 1, and the height and extent of siltation downstream of pier NO. 6 also increased significantly. These findings indicate that the presence of the quasi-stumps group was highly beneficial for the stability of the

bridge piers. The main reason why the quasi-stumps group could change the erosion and deposition patterns around the piers was that this structure could effectively reduce its downstream flow velocities, so that the suspended sediment originally moving with the flow could be deposited on the riverbed. Meanwhile, the shear stress of the flow on the riverbed was decreased due to the decrease in the flow velocities, thus weakening the scouring effect on the riverbed. Therefore, under the dual effect of promoting siltation and weakening scouring, the riverbed around the piers gradually formed siltation.

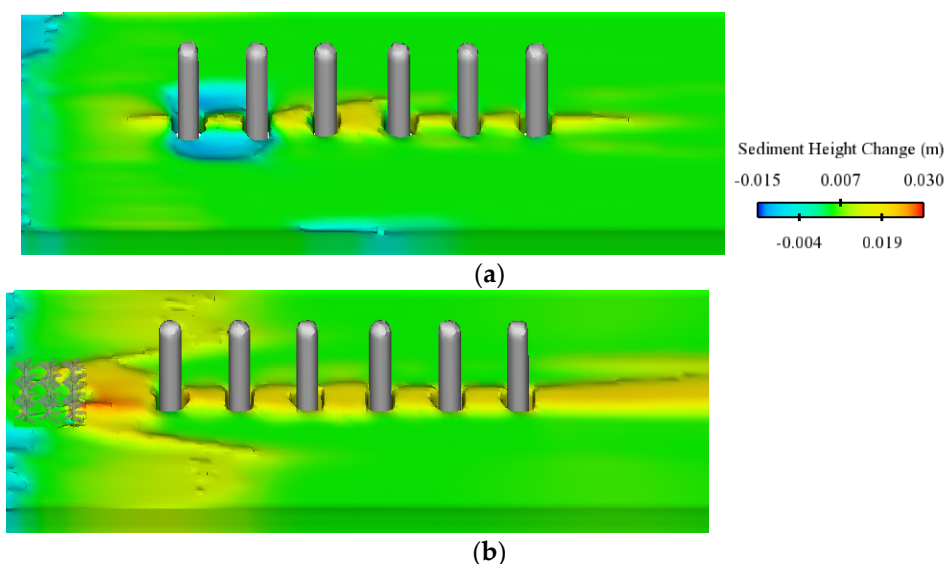


Figure 14. Comparison of the three-dimensional riverbed topography around the piers after erosion and sedimentation without (a) and with (b) the quasi-stumps group. (a) Without the protection of the quasi-stumps group. (b) With the protection of the quasi-stumps group.

During the whole experiment, the quantities of suspended sediment deposition in experiment NO. 0 (without quasi-stumps group) and experiment NO. 3 (with quasi-stumps group) were 3.69 kg and 9.16 kg, respectively. The latter was 2.48 times more than the former, indicating that the quasi-stumps group effectively promoted the deposition of suspended sediment. In experiments NO. 0 and NO. 3, the quantities of sediment scoured from the riverbed were 8.25 kg and 1.75 kg, respectively. It was observed that the former was 4.71 times greater than the latter. This indicates that the quasi-stumps group effectively weakens the erosion on the riverbed.

The increase in suspended sediment deposition and the decrease in sediment scoured from the riverbed were mainly attributed to the quasi-stumps group that could effectively lower the flow velocities around piers. Measurements of the flow velocities around the piers were taken, and the locations of the measurement points are shown in Figure 11. The flow velocity at each point both without (experiment NO. 0) and with (experiment NO. 3) the quasi-stumps group is shown in Figure 15, and all the points are located at one-fourth the water depth. Based on Figure 15, it is evident that the flow velocities around the piers with the quasi-stumps group were significantly lower than those without the quasi-stumps group.

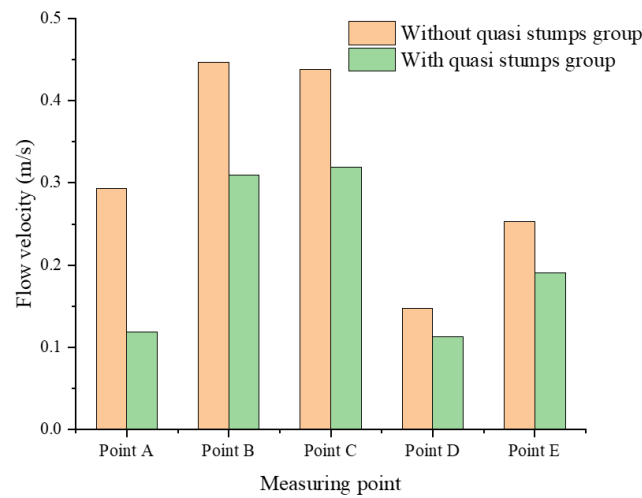


Figure 15. Comparison of the flow velocity at each point around the piers with and without the quasi-stumps group.

3.3. The effect of Horizontal Distance L on Siltation Characteristics

The distance between the quasi-stumps group and the piers significantly impacted the sediment deposition around the piers. After each experiment, the bed topographic elevation along the centerline of the piers was measured using a needle water level gauge. Figure 16 shows the longitudinal section of the riverbed topography along the centerline (along the flow direction) of the piers group at different distances L . At the initial time, the height of the riverbed was 0.12 m. As the value of L increased, the siltation height of both the upstream and downstream areas of the piers decreased gradually. Additionally, the reduction in flow velocities around the piers became less significant as the quasi-stumps group moved farther away from the piers. As a result, the deposition of the suspended sediment decreased. There was no erosion around the piers. Starting from pier NO. 1, the deposition height gradually decreased with the increasing X . The average deposition height for $L = 5D, 4D, 3D,$ and $2D$ were 0.824, 0.878, 0.920, and 0.966 times that for $L = D$, respectively.

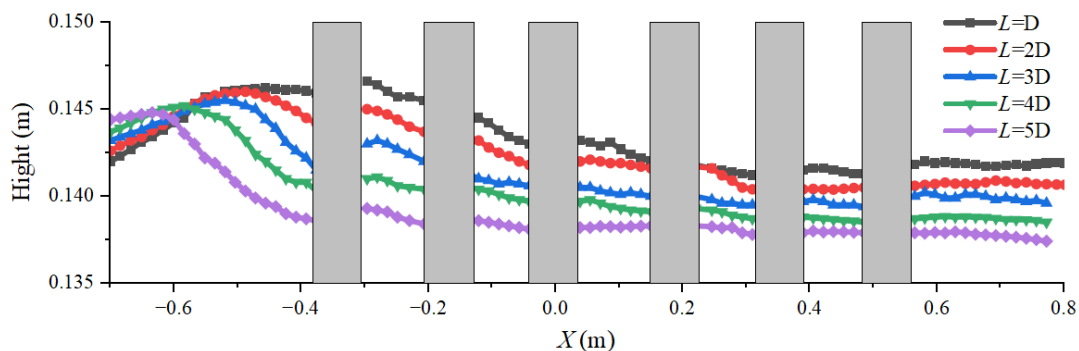


Figure 16. The longitudinal section of the riverbed along the centerline of the piers group at different L .

Figure 17 shows the siltation on the left side along the centerline of pier NO. 1 (perpendicular to the flow direction) at different distances L . As the value of L increases, the siltation height on both sides of pier NO. 1 gradually decreases, and the degree of change near the pier ($Y = 0.03\text{--}0.18$ m) is greater than that away from the pier ($Y = 0.18\text{--}0.36$ m). At the same L , the deposition height away from the pier is greater than that near the pier. This is due to the velocities and fluctuations of the flow near the pier that are higher than those farther away from the pier. From Figure 17, it can be observed that there are irregular variations in the sedimentation height in the areas far from the bridge piers. This is mainly

because the quasi-stumps group has less influence on the flow velocities and sediment movements in the area away from the pier compared to the area near the pier.

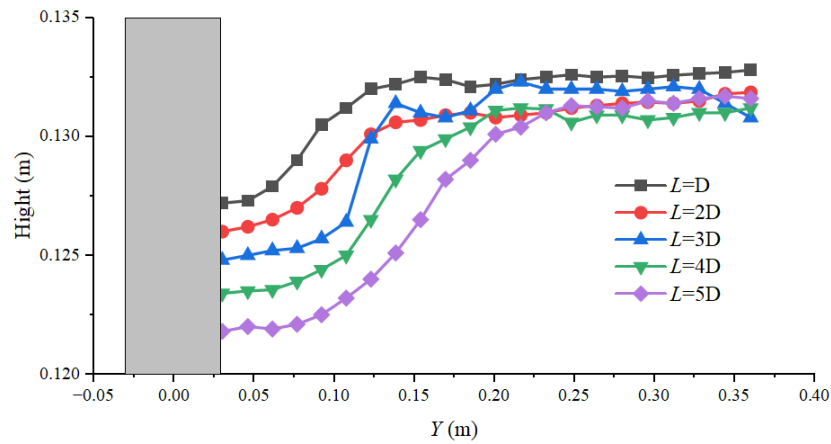


Figure 17. A cross-section of the riverbed along the centerline of pier NO. 1 on the left side at different L .

Figure 18 shows the variations in the dimensionless maximum deposition height d_h/D and deposition area A_h/A_D with the distance L . With the increase of L , the maximum deposition height decreases slowly, and the deposition area increases gradually. The average growth rates of the maximum deposition height and deposition area are -1.79% and 6.43% , respectively. The influence of L on the maximum deposition height is insignificant. The closer the quasi-stumps group is situated to the inlet, the greater the range of downstream velocity reduced by it, resulting in an increased deposition of the suspended sediment in the downstream area. Consequently, the deposition area also increases, albeit within a relatively small range of change.

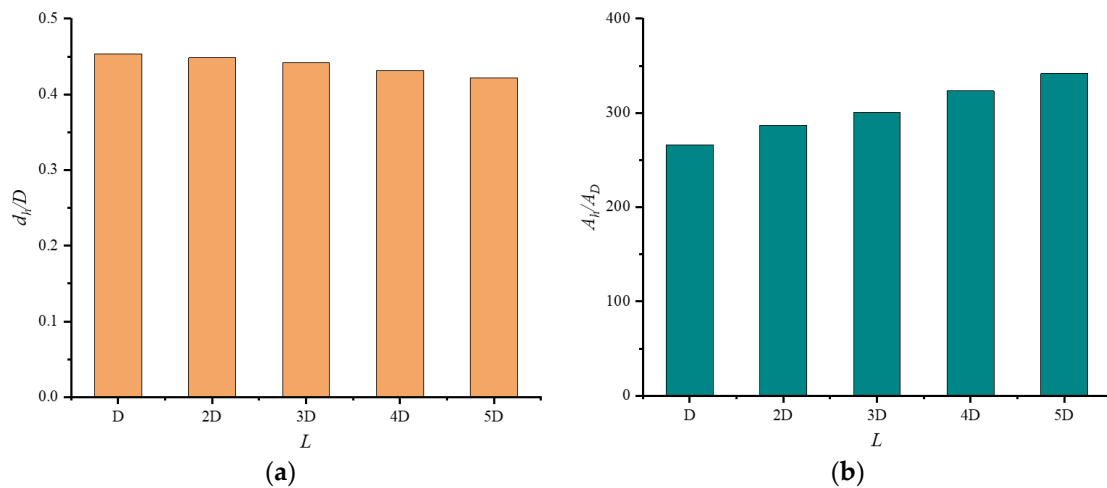


Figure 18. The change in the dimensionless maximum siltation height (a) and siltation area (b) with L . (a) Maximum siltation height. (b) Siltation area.

The quantity of sediment scoured from the riverbed and the quantity of suspended sediment deposition during the experiment vary with the distance L , as shown in Figure 19, and the duration of the experiment is one hour. From Figure 19, it is evident that the quantity of suspended sediment deposition is significantly greater than the quantity of sediment scoured from the riverbed. As the distance L increases, the quantity of suspended sediment deposition increases gradually, the quantity of sediment scoured from the riverbed decreases gradually, and their average growth rates are 9.69% and -4.01% , respectively. The total sediment in the riverbed increases with an increase in L , which is consistent with the previously observed

variation of siltation area with L . On average, the quantity of suspended sediment deposition is 5.25 times greater than the quantity of sediment scoured from the riverbed.

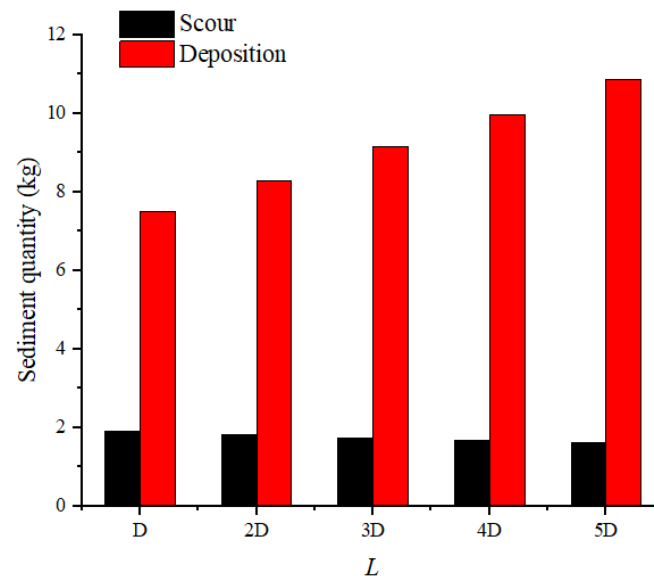


Figure 19. The variation in sediment scoured from the riverbed, and the deposition of suspended sediment with L .

The primary cause for alterations in the deposition height, deposition area, and sediment quantity is attributed to the changes in the flow velocities around the piers. Therefore, the flow velocities at various points around the piers under different distances L were measured. All points are situated at one-fourth the water depth. The changes in the flow velocity at each point concerning L are shown in Figure 20. Based on Figure 20, it is evident that the flow velocity of each point increases with an increase in L , and the change at point A is the largest. Points B and C have similar velocities, which are the highest among the five points. Points D and E are less affected by the changes in L . From Figures 19–21, it can be observed that, as L increases, the flow velocities at points A, B, C, D, and E gradually increase. However, at the same time, the deposition area and the deposited sediment also increase. This is mainly due to the change in location of the quasi-stumps group. The sedimentation is more significantly influenced by the position of the quasi-stumps group. As L increases, the closer the quasi-stumps group is to the flow inlet, and the larger the area in the flume where the flow velocities are reduced due to the presence of the quasi-stumps group; therefore, more sediment is deposited. Although the flow velocity at each point increases with the increase in L , all the flow velocities are reduced relative to the inlet flow velocity of 0.48 m/s.

3.4. The Effect of the Height P of the Quasi-Stumps Group on Siltation Characteristics

The movement of the sediment around the piers will be influenced by the height P of the quasi-stumps group. Figure 21 shows the longitudinal section of the riverbed topography at different heights P along the centerline of the piers group. With the increase in height P , the siltation height gradually increases. This is due to the enhanced ability of the quasi-stumps group to reduce the flow velocities and intercept the suspended sediment, leading to more suspended sediment being deposited downstream. The maximum siltation height occurs in the region between the quasi-stumps group and pier NO. 1. The average siltation height for $P = 2H/3$ and $P = H$ is 1.081 and 1.166 times higher than that for $P = H/3$, respectively.

Figure 22 shows the siltation height along the left side of the centerline of pier NO. 1 at different heights P . The siltation height gradually increases with the increase in P , and the changes in the area ($Y = 0.03$ – 0.12 m) near the pier are greater.

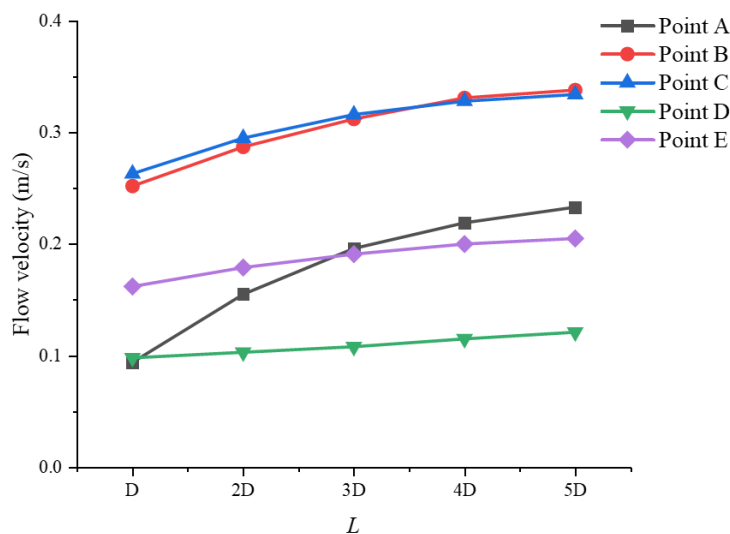


Figure 20. The variation of the flow velocities at five points around the piers with L .

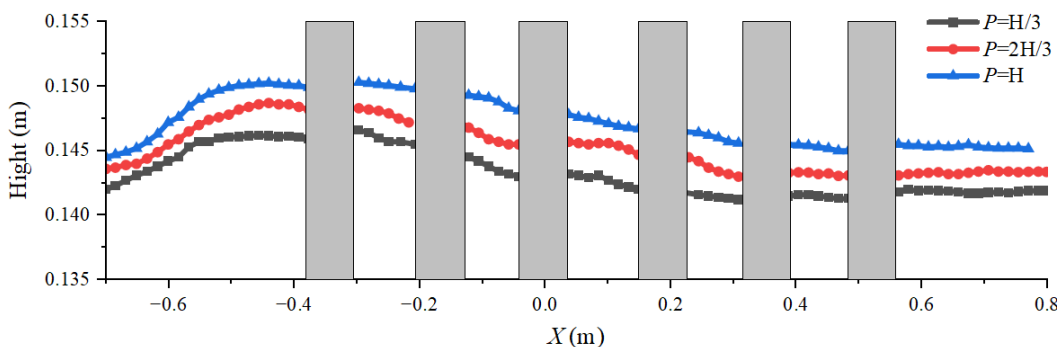


Figure 21. The longitudinal section of the riverbed along the centerline of the piers group at different P .

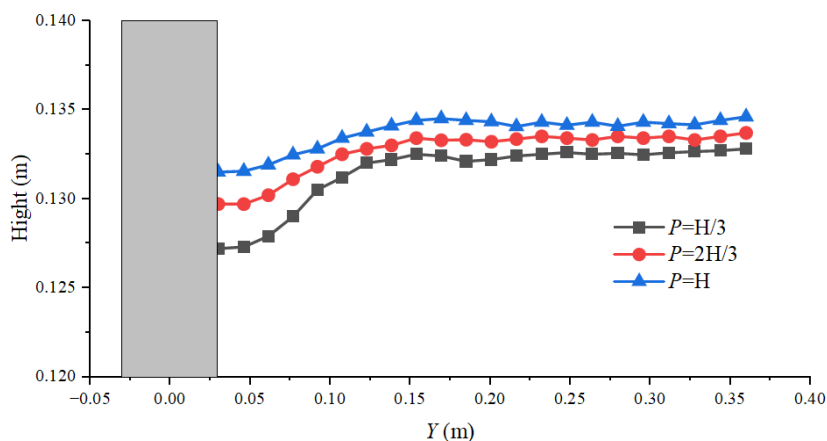


Figure 22. The cross-section of the riverbed along the centerline of pier NO. 1 on the left side at different P .

The dimensionless maximum siltation height d_h/D and siltation area A_h/A_D vary with the height P , as shown in Figure 23. It is observed that both the maximum siltation height and siltation area gradually increase with the increase in P , and their average growth rates are 6.77% and 18.55%, respectively. Notably, the siltation area appears to be more significantly influenced by the height of the quasi-stumps group than the maximum siltation height.

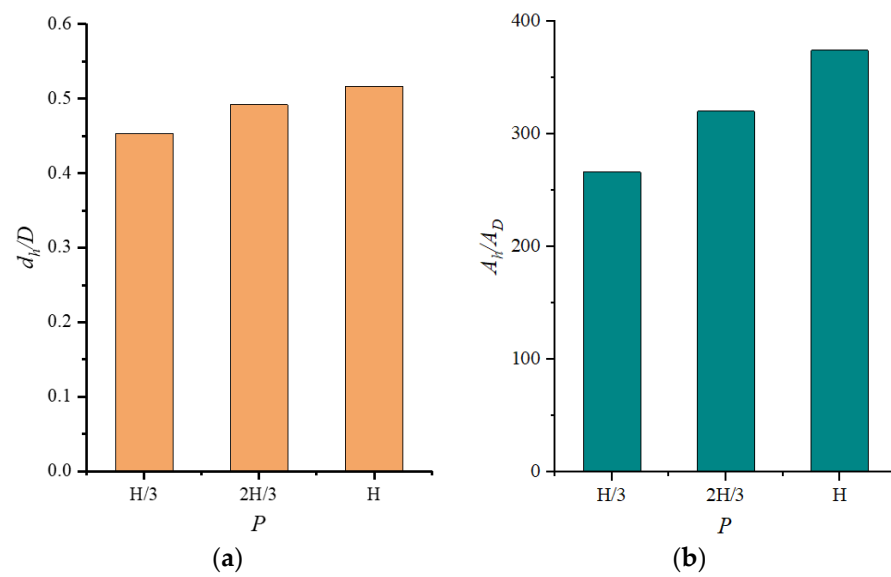


Figure 23. The change in the dimensionless maximum siltation height (a) and siltation area (b) with the P . (a) Maximum siltation height. (b) Siltation area.

During the experiment, the quantity of sediment scoured from the riverbed and the quantity of suspended sediment deposition vary with the height P , as shown in Figure 24. With the increase in height P , the quantity of sediment scoured from the riverbed gradually decreases, the quantity of suspended sediment deposition gradually increases, and their average growth rates are -6.18% and 24.59% , respectively. The height P has a significant impact on both, especially the deposition of the suspended sediment. On average, the quantity of the suspended sediment deposition is 5.39 times greater than the quantity of sediment scoured from the riverbed. Therefore, the ability of the quasi-stumps group to promote the deposition of the suspended sediment is significantly impacted by its height.

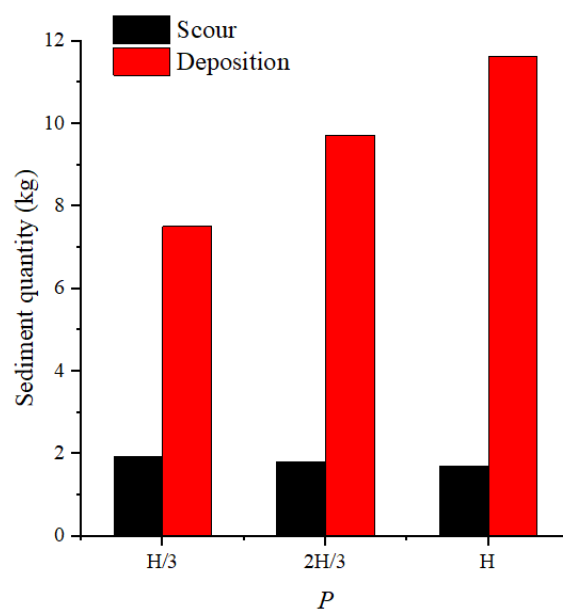


Figure 24. The variations in sediment scoured from the riverbed, and the deposition of the suspended sediment with the P .

The flow velocities of points around the bridge piers under different heights P were measured, and all points were located at half the depth of the water. The selection of half of the water depth was to better demonstrate the influence of the height of the quasi-stumps group on the flow velocities, as the heights of the quasi-stumps group were one-third of the water depth, two-thirds of the water depth, and equal to the water depth. The variations in the flow velocity at each point with L are shown in Figure 25. The flow velocity at each point decreases with the increase in height P , but the degree in decrease is different. Among them, the changes of points D and E are the smallest, and the flow velocities of points B and C are similar. When P is increased from $H/3$ to $2H/3$, there is a significant decrease in the flow velocities observed at point A. This is due to the fact that the height of the quasi-stumps group changes from being below point A to being above it during this process. As the height P increases, the flow velocity decreases at various points around the piers, leading to a gradual increase in the maximum siltation height, siltation area, and quantity of the sediment deposition. This outcome is rational and in accordance with expected trends.

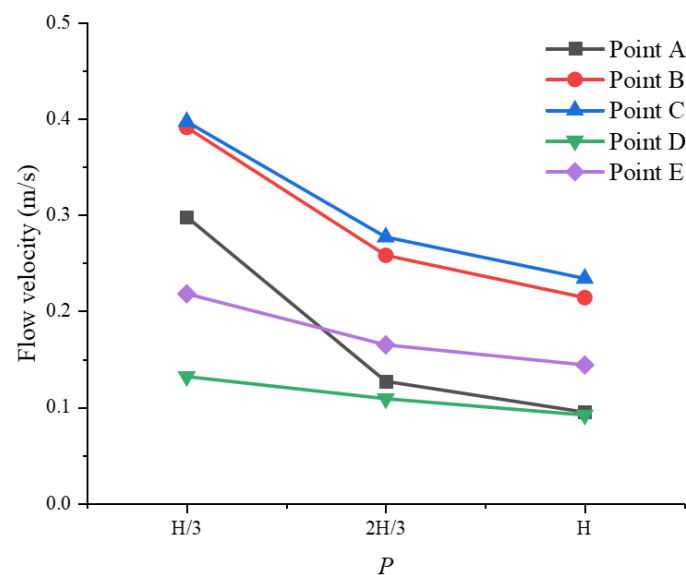


Figure 25. The variations in the flow velocities at five points around the piers with the P .

3.5. The Effect of the Ratio S between the Single Leaf Area and the Cross-Sectional Area of Single Pier on the Siltation Characteristics

The siltation around the bridge piers is influenced by the area of leaves in the quasi-stumps group. S represents the ratio of the area of a single leaf to the cross-sectional area of a single pier. Figure 26 shows the riverbed topography along the centerline of the piers group in a longitudinal section at different S . The siltation heights both upstream and downstream of the piers gradually increase with the increase in S . This indicates that, the larger the single leaf area, the stronger the ability of this structure to promote sediment deposition. The locations of the highest siltation points are nearly identical for different values of S . The average deposition heights for $S = 0.148, 0.133, 0.118,$ and 0.103 are 1.156, 1.124, 1.079, and 1.034 times higher than $S = 0.088$, respectively.

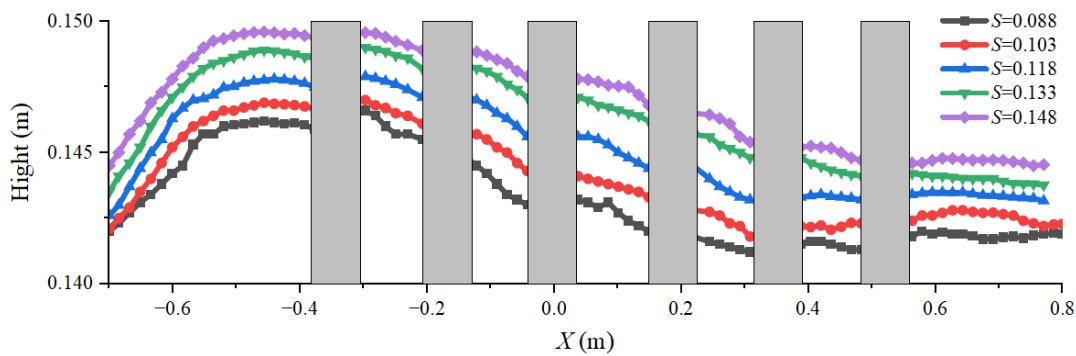


Figure 26. The longitudinal section of the riverbed along the centerline of the piers group at different S .

The data in Figure 27 demonstrate the height of siltation along the left side of the centerline of pier NO. 1 at different ratios S . The siltation height gradually increases with the increase in S . The deposition height of the riverbed close to the pier ($Y = 0.03–0.15$ m) is comparatively lower than that of the riverbed farther away from the pier ($Y = 0.15–0.36$ m). When $S = 0.148$, the siltation height at each point along the left side of the pier is approximately equal.

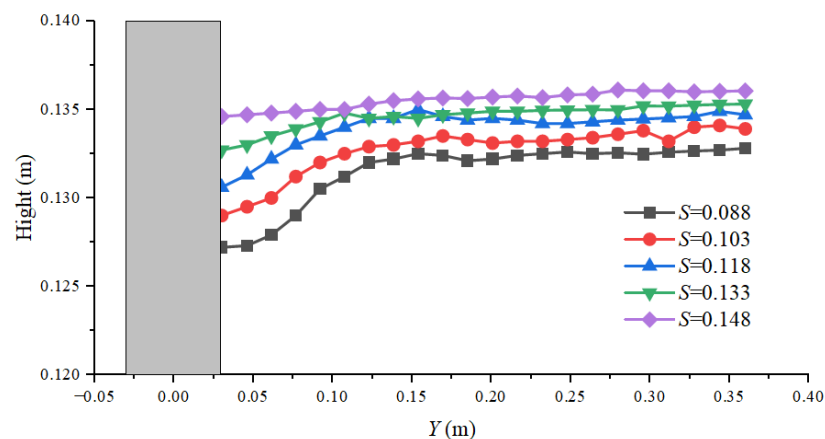


Figure 27. The cross-section of the riverbed along the centerline of pier NO. 1 on the left side at different S .

Figure 28 shows the variations of the dimensionless maximum siltation height d_h/D and siltation area A_h/A_D with the S . The results indicate that both the maximum siltation height and siltation area gradually increase with the increase in S . Their average growth rates are 2.66% and 10.0%, respectively. The effect of the single leaf area on the maximum siltation height is very small.

The quantity of sediment scoured from the riverbed and the quantity of suspended sediment deposition during the experiment vary with the ratio S , as shown in Figure 29. As the value of S increases, the quantity of sediment scoured from the riverbed decreases gradually, and the quantity of the suspended sediment deposition increases gradually. Their average growth rates are -7.58% and 10.22% , respectively. Furthermore, the mass of the suspended sediment deposition is, on average, 5.77 times greater than the mass of sediment scoured from the riverbed.

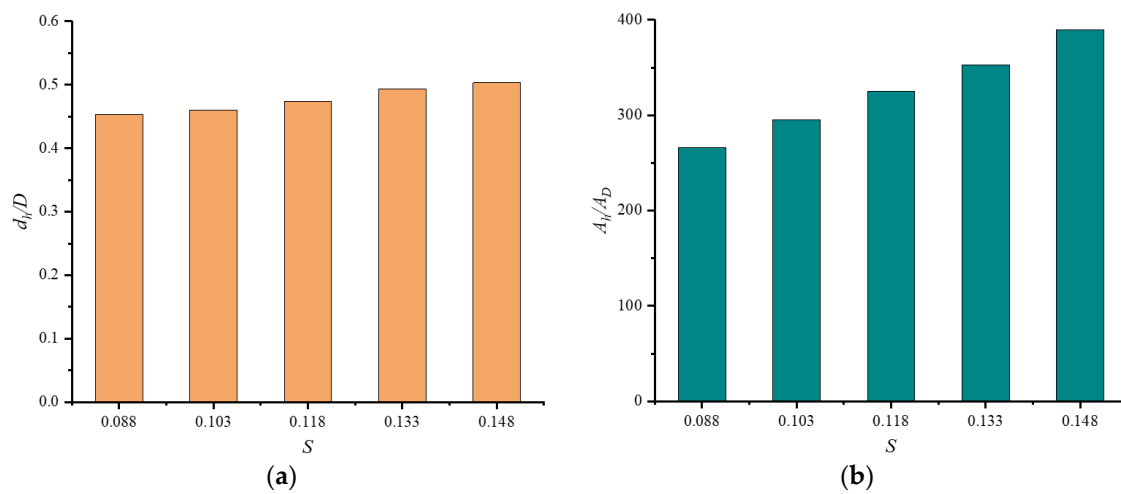


Figure 28. The changes in the dimensionless maximum siltation height (a) and siltation area (b) with the S. (a) Maximum siltation height. (b) Siltation area.

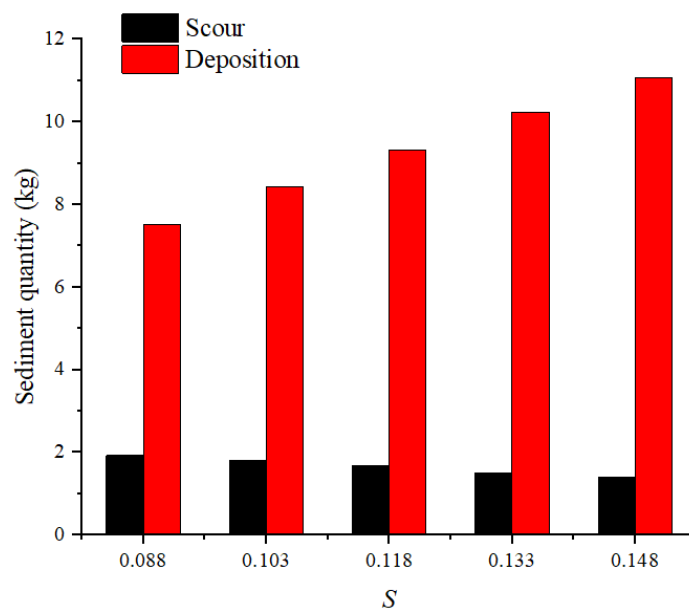


Figure 29. The variations in the sediment scoured from the riverbed and the deposition of the suspended sediment with the S.

During the experiment, the flow velocities around the piers were measured, and the measurement point locations are illustrated in Figure 11, where each point is posited at one-fourth the water depth. Figure 30 illustrates the variations in the the flow velocity at each point with the S. As the S increases, the flow velocities of all the points decrease. The most significant change is observed at point A, and the smallest change is noted at points D and E. These findings are consistent with the results of the variations in the siltation height, siltation area, and mass of the sediment on the riverbed with the S.

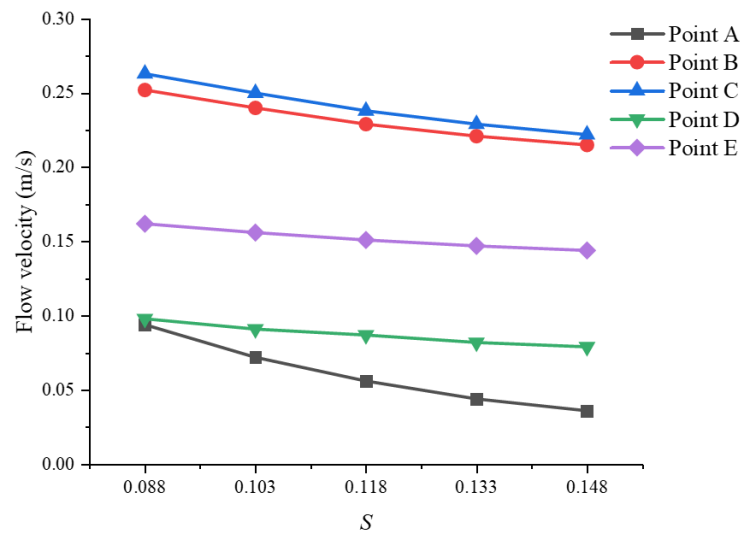


Figure 30. The variations in the flow velocities at five points around the piers with the S .

4. Discussion

The shapes of the scour holes around the piers are shown in Figure 14a, and they are different from the shapes of the scour holes obtained by Daneshfaraz et al. [42] and Kim et al. [43] through experiments, who believed that the riverbed upstream of the first pier should be scoured. However, as can be seen from Figure 14a, the riverbed upstream of the first pier was not scoured, but a small amount of sediment siltation was formed. This was mainly due to the RNG $k-\epsilon$ turbulence model used in the numerical simulation of this study, and the inlet flow was the carrying flow with a sediment content of 2.7 kg/m^3 . The cross-section of the riverbed at the $Y = 0$ plane is shown in Figure 31, where the solid black line represents the original riverbed surface. It can be observed from the figure that the riverbed upstream of pier NO. 1 was not all silted up, and the scour pit was formed within a range 2.3 cm upstream of this pier. The scour pit is shown in the red dotted box in Figure 31.

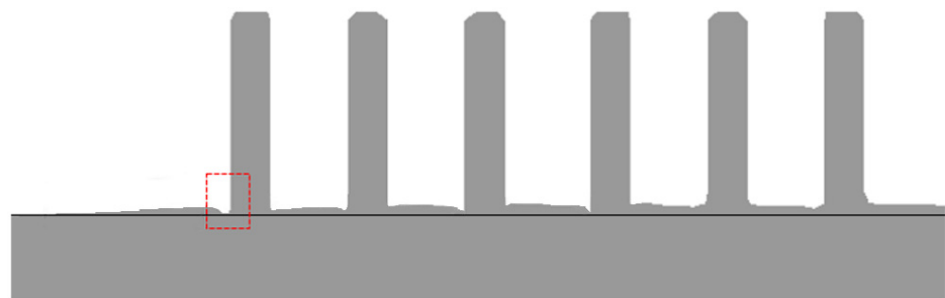


Figure 31. The height of the riverbed on the $Y = 0$ plane for experiment NO. 0.

The Reynolds-averaged Navier–Stokes equation model (RANS) cannot effectively capture the high-energy turbulent eddies at the junction between the upstream face of the bridge pier and the riverbed, which will cause the riverbed erosion upstream of the pier to be less than the actual situation [44]. The RNG $k-\epsilon$ turbulence model used in this study, as a kind of Reynolds-averaged Navier–Stokes model, also has this problem. Many simulation results based on RANS models exhibit this same phenomenon as well. For instance, Wang et al. [45] calculated the scour holes around a pier using the RNG $k-\epsilon$ turbulence model, as shown in Figure 32a. Li et al. [46] obtained the scour holes at a flow velocity of 0.4 m/s using the $k-\omega$ turbulence model, as shown in Figure 32b. ω is also the turbulence dissipation rate, which represents the rate of energy dissipation in a turbulent flow. In a turbulent flow, vortices are continuously generated and dissipated, leading to

energy conversion and dissipation during this process. Compared to the k - ϵ turbulence model, the k - ω turbulence model solves for a specific rate ω of kinetic energy dissipation, and it is a low Reynolds number model. Its nonlinearity is greater, making it more difficult to converge, and it is quite sensitive to the initial guess of the solution. The k - ϵ turbulence model performs well in many common turbulent flow fields, while the k - ω turbulence model is more suitable for simulating rotational flows. Wang et al. [44] obtained the scour hole using the realizable k - ϵ turbulence model, as shown in Figure 32c.

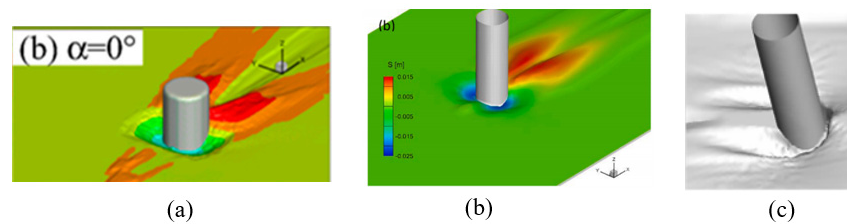


Figure 32. The scour pits obtained by other researchers: (a) Ref. [45]; (b) Ref. [46]; (c) Ref. [44].

The streamlines around the first and second piers of experiment NO. 0 are shown in Figure 33, which are similar to the streamlines of the longitudinal section obtained by Li et al. [47]. It can be observed from the figure that the streamlines upstream of the first pier are smoother, so the erosion effect of the flow on the riverbed is small. Figure 34 shows the velocity nephogram on the plane of $Z = 0.15$ m. The flow velocities in the area upstream of the first pier are reduced, as shown in the red box in Figure 34, which allows some of the suspended sediment located at the bottom of the flow to be deposited there.

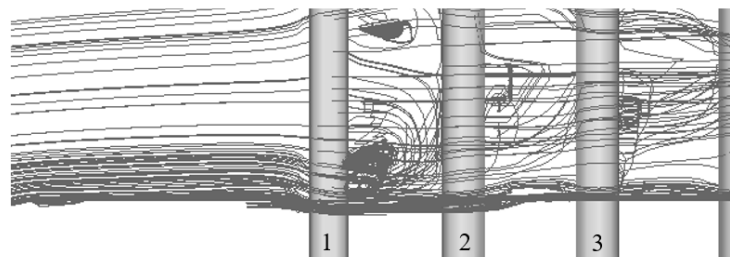


Figure 33. The streamlines around the piers in experiment NO. 0.

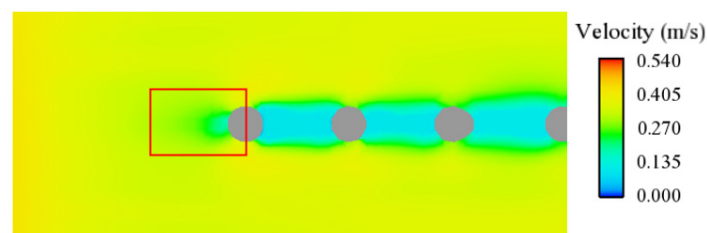


Figure 34. The velocity nephogram of experiment NO. 0 on the plane of $Z = 0.15$ m.

For experiments NO. 1 to 11 with the protection of the quasi-stumps group, the main reason for the significant accumulation of sediment around the piers is that the quasi-stumps group can effectively reduce the downstream flow velocities, thus weakening the shear stress of the flow on the riverbed and promoting the deposition of more suspended sediment around the piers. Additionally, the sediment concentration in the water downstream of the quasi-stumps group is higher than that of the inlet flow due to the decrease in the flow velocities. The presence of suspended sediment in the flow will reduce the shear stress on the riverbed and diminish the turbulence within the flow [48] and further reduce the erosion of the riverbed by the flow.

The flow field and scour around the group of bridge piers are very complex and influenced by numerous factors, such as the flow velocity, sediment particle size and gradation, distance between piers, angle between the piers group and the flow direction, water depth, and more. The current study in this paper is very limited and only investigates the effects of the quasi-stumps group and its L , P , and S on the siltation characteristics around the piers group. Many of the initial conditions in this study are predefined and remain unchanged. In future research, the initial conditions can be modified, and the effects of these initial conditions on the scour and siltation can be analyzed to better understand the scour mechanism of a riverbed around bridge piers.

5. Conclusions

In this study, both experiments and numerical simulations using FLOW 3D were employed to examine the protective effect of a quasi-stumps group on the local scour of bridge piers. Specifically, the scour and deposition of the riverbed around the piers, as well as the flow velocities, were compared under two conditions: with and without the quasi-stumps group. Three factors affecting the protective effect of the quasi-stumps group were studied: the horizontal distance L between the quasi-stump group and the pier, the height P of the quasi-stumps group, and the ratio S of the area of a single leaf on the quasi-stumps group to the cross-sectional area of a single pier. The effects of various factors on the siltation height at the centerline of the piers, the maximum siltation height, the siltation area, the change in quantity of the bedload sediment and suspended sediment, and the flow velocities around the piers were analyzed. The results are as follows:

- (1) The results of the numerical simulations using FLOW 3D are in good agreement with the experimental results.
- (2) The presence of the quasi-stumps group can effectively lower the flow velocities around the piers, promote the deposition of suspended sediment, and reduce the sediment scoured from the riverbed. It does not only help safeguard the riverbed around the piers against scouring but also forms siltation, which is beneficial to the stability of the bridge piers.
- (3) As the distance L increases, the siltation height at the centerline of the piers group decreases gradually. However, the siltation area and the quantity of the suspended sediment deposition on the entire riverbed gradually increase.
- (4) With the increase in the height P and ratio S , the siltation height at the centerline of the piers group, the maximum siltation height, the siltation area, and the quantity of the suspended sediment deposition gradually increase, while the flow velocities around the piers gradually decrease.
- (5) The quantity of sediment scoured from the riverbed is less influenced by the L , P , and S .
- (6) In this study, the combination of the quasi-stumps group with the best protective effect is $P = H$, $S = 0.148$, and $L = D$.

Author Contributions: Data curation, J.W. and W.T.; Supervision, Y.C.; Investigation, J.W. and W.T.; Software, Q.Z. and W.T.; Methodology, Y.Z.; Visualization, Y.C.; and Writing—review and editing, Y.Z. All authors have read and agreed to the published version of the manuscript.

Funding: This research received no external funding.

Data Availability Statement: The data that support the findings in this study are available from the corresponding author upon reasonable request.

Conflicts of Interest: The authors declare no conflict of interest.

Appendix A

The meanings of the symbols used in this paper are as follows:

Symbol	Meaning
D	Pier diameter
V	Average velocity upstream of the pier
H	Water depth
d_m	Maximum scouring depth
d_a	Average scouring depth
d_h	Maximum deposition height
A_h	Deposition area
A_D	Cross-sectional area of a single pier
S	Ratio of the area of a single leaf to the cross-sectional area of a single pier
P	Height of the stumps group in the water
L	Horizontal distance between the downstream edge of the stumps group and the upstream edge of Pier NO. 1
RANS	Abbreviation of the Reynolds-averaged Navier–Stokes equation model
RNG	Abbreviation of renormalization group
k	Turbulent kinetic energy of the turbulence model
ε	Turbulent dissipation rate of the k - ε turbulence model
ω	Turbulent dissipation rate of the k - ω turbulence model
X, Y, Z	Coordinate values in the x, y , and z directions of the coordinate axes are shown in Figure 5a

References

- Smith, D.W. Why do bridges fail? *Civ. Eng.* **1977**, *47*, 58–62.
- Lagasse, P.F.; Clopper, P.E.; Zevenbergen, L.W.; Girard, L.G. *NCHRP Report 593: Countermeasures to Protect Bridge Piers from Scour*; Transportation Research Board: Washington, DC, USA, 2007.
- Arneson, L.A.; Zevenbergen, L.W.; Lagasse, P.F.; Clopper, P.E. *Evaluating Scour at Bridges*, 5th ed.; Bridge Superstructures; U.S. Department of Transportation: Washington, DC, USA, 2012.
- Chiew, Y.M. Scour protection at bridge piers. *J. Hydraul. Eng. ASCE* **1992**, *118*, 1260–1269. [[CrossRef](#)]
- Wang, C.; Yu, X.; Liang, F.Y. A review of bridge scour: Mechanism, estimation, monitoring and countermeasures. *Nat. Hazards* **2017**, *87*, 1881–1906. [[CrossRef](#)]
- Jalal, H.K.; Hassan, W.H. Effect of Bridge Pier Shape on Depth of Scour. *IOP Conf. Ser. Mater. Sci. Eng.* **2020**, *671*, 12001. [[CrossRef](#)]
- Jahangirzadeh, A.; Basser, H.; Akib, S.; Karami, H.; Naji, S.; Shamshirband, S. Experimental and Numerical Investigation of the Effect of Different Shapes of Collars on the Reduction of Scour around a Single Bridge Pier. *PLoS ONE* **2014**, *9*, e98592. [[CrossRef](#)] [[PubMed](#)]
- Nazari-Sharabian, M.; Nazari-Sharabian, A.; Karakouzian, M.; Karami, M. Sacrificial Piles as Scour Countermeasures in River Bridges a Numerical Study using FLOW-3D. *Civ. Eng. J.* **2020**, *6*, 1091–1103. [[CrossRef](#)]
- Dey, S.; Sumer, B.M.; Fredsoe, J. Control of scour at vertical circular piles under waves and current. *J. Hydraul. Eng.* **2006**, *132*, 270–279. [[CrossRef](#)]
- Kumar, V.; Raju, K.G.R.; Vittal, N. Reduction of local scour around bridge piers using slots and collars. *J. Hydraul. Eng. ASCE* **1999**, *125*, 1302–1305. [[CrossRef](#)]
- Mou, X.; Wang, D.; Ji, H.; Li, C.; Qiao, C. Resistance capability and hydraulic characteristics of ring-wing plates against local scour of round-ended piers. *South North Water Transf. Water Sci. Technol.* **2017**, *15*, 146–155. [[CrossRef](#)]
- Zhang, Y.S.; Wang, J.F.; Zhou, Q.; Li, H.S.; Tang, W. Investigation of the reduction of sediment deposition and river flow resistance around dimpled surface piers. *Environ. Sci. Pollut. Res.* **2023**, *20*, 52784–52803. [[CrossRef](#)]
- Chiew, Y.M. Mechanics of riprap failure at bridge piers. *J. Hydraul. Eng. ASCE* **1995**, *121*, 635–643. [[CrossRef](#)]
- Parola, A.C.; Mahavadi, S.K.; Brown, B.M.; ElKhoury, A. Effects of rectangular foundation geometry on local pier scour. *J. Hydraul. Eng. ASCE* **1996**, *122*, 35–40. [[CrossRef](#)]
- Li, Z.; Tang, H.; Dai, W. Case study of protective effects of ripraps or tetrahedron frame group with different densities on local scour around a pier. *J. Sediment Res.* **2011**, *6*, 75–80. [[CrossRef](#)]
- Jones, J.S.; Kilgore, R.T.; Mistichelli, M.P. Effects of footing location on bridge pier scour. *J. Hydraul. Eng. ASCE* **1992**, *118*, 280–290. [[CrossRef](#)]
- Shilong, F.; Hongwu, T.; Yilin, Z.; Kaixi, C.A.I. Experimental study on effect of local scour at piers and protection by tetrahedron frame. *Adv. Water Sci.* **2006**, *17*, 354–358. [[CrossRef](#)]
- Tabarestani, M.K.; Zarrati, A.R. Design of Stable Riprap around Aligned and Skewed Rectangular Bridge Piers. *J. Hydraul. Eng.* **2013**, *139*, 911–916. [[CrossRef](#)]
- Melville, B.W. Live-bed scour at bridge piers. *J. Hydraul. Eng. ASCE* **1984**, *110*, 1234–1247. [[CrossRef](#)]
- Abt, S.R.; Clary, W.P.; Thornton, C.I. Sediment deposition and entrapment in vegetated streambeds. *J. Irrig. Drain. Eng. ASCE* **1994**, *120*, 1098–1111. [[CrossRef](#)]

21. Sun, Z.L.; Zheng, J.Y.; Zhu, L.L.; Chong, L.; Liu, J.; Luo, J.Y. Influence of submerged vegetation on flow structure and sediment deposition. *J. Zhejiang Univ. Eng. Sci.* **2021**, *55*, 71–80. [[CrossRef](#)]
22. Nabaei, S.F.; Afzalimehr, H.; Sui, J.Y.; Kumar, B.; Nabaei, S.H. Investigation of the Effect of Vegetation on Flow Structures and Turbulence Anisotropy around Semi-Elliptical Abutment. *Water* **2021**, *13*, 3108. [[CrossRef](#)]
23. Amir, M.; Hashmi, H.N.; Baloch, M.; Ehsan, M.A.; Muhammad, U.; Ali, Z. Experimental investigation of channel bank vegetation on scouring characteristics around a wing wall abutment. *Mehran Univ. Res. J. Eng. Technol.* **2018**, *23*, 16–22.
24. Wang, H.; Tang, H.; Zhao, H.; Zhao, X.; Lu, S. Incipient motion of sediment in presence of submerged flexible vegetation. *Water Sci. Eng.* **2015**, *8*, 63–67. [[CrossRef](#)]
25. Hongwu, T.; Shengqi, L.U.; Jianchuan, L. Settling velocity of coarse sediment particles in still water with rigid vegetation. *J. Hydraul. Eng.* **2007**, *38*, 1214–1220. [[CrossRef](#)]
26. Zhao, H.Q.; Yan, J.; Yuan, S.Y.; Liu, J.F.; Zheng, J.Y. Effects of Submerged Vegetation Density on Turbulent Flow Characteristics in an Open Channel. *Water* **2019**, *11*, 2154. [[CrossRef](#)]
27. Xiong, W.; Tang, P.B.; Kong, B.; Cai, C.S. Computational Simulation of Live-Bed Bridge Scour Considering Suspended Sediment Loads. *J. Comput. Civ. Eng.* **2017**, *31*, 12. [[CrossRef](#)]
28. Yu, S.L.; Dai, H.C.; Zhai, Y.W.; Liu, M.Y.; Huai, W.X. A Comparative Study on 2D CFD Simulation of Flow Structure in an Open Channel with an Emerged Vegetation Patch Based on Different RANS Turbulence Models. *Water* **2022**, *14*, 2873. [[CrossRef](#)]
29. Chen, M.; Lou, S.; Radnaeva Larisa, D.; Nikitina, E.; Chalov Sergey, R. Numerical Simulation of Wave Propagation and Sediment Suspension Affected by Submerged Rigid Vegetation. *J. Tongji Univ. Nat. Sci.* **2022**, *50*, 861–870. [[CrossRef](#)]
30. Asadollahi, M.; Vaghefi, M.; Akbari, M. Effect of the position of perpendicular pier groups in a sharp bend on flow and scour patterns: Numerical simulation. *J. Braz. Soc. Mech. Sci. Eng.* **2020**, *42*, 422. [[CrossRef](#)]
31. Bozkus, Z.; Ozalp, M.C.; Dincer, A.E. Effect of Pier Inclination Angle on Local Scour Depth Around Bridge Pier Groups. *Arab. J. Sci. Eng.* **2018**, *43*, 5413–5421. [[CrossRef](#)]
32. Heidarpour, M.; Afzalimehr, H.; Izadinia, E. Reduction of local scour around bridge pier groups using collars. *Int. J. Sediment Res.* **2010**, *25*, 411–422. [[CrossRef](#)]
33. Saghravani, S.F.; Azhari, A. Simulation of clear water local scour around a group of bridge piers using an Eulerian 3D, two-phase model. *Prog. Comput. Fluid Dyn.* **2012**, *12*, 333–341. [[CrossRef](#)]
34. Voskoboinick, A.; Voskoboinick, V.; Turick, V.; Voskoboinyk, O.; Cherny, D.; Tereshchenko, L. Interaction of Group of Bridge Piers on Scour. In *Advances in Computer Science for Engineering and Education III. Advances in Intelligent Systems and Computing (AISC 1247)*; Springer: Berlin/Heidelberg, Germany, 2021; pp. 3–17. [[CrossRef](#)]
35. Jahangirzadeh, A.; Akib, S. Experimental study for determination of collar dimensions around bridge pier. *Balt. J. Road Bridge Eng.* **2015**, *10*, 89–96. [[CrossRef](#)]
36. Obied, N.A.; Khassaf, S.I. Experimental Study for Protection of Piers Against Local Scour Using Slots. *Int. J. Eng.* **2019**, *32*, 217–222. [[CrossRef](#)]
37. Debnath, K.; Chaudhuri, S. Effect of suspended sediment concentration on local scour around cylinder for clay-sand mixed sediment beds. *Eng. Geol.* **2011**, *117*, 236–245. [[CrossRef](#)]
38. Chiew, Y.M.; Melville, B.W. Local scour around bridge piers. *J. Hydraul. Res.* **1987**, *25*, 15–26. [[CrossRef](#)]
39. Mastbergen, D.R.; van den Berg, J.H. Breaching in fine sands and the generation of sustained turbidity currents in submarine canyons. *Sedimentology* **2003**, *50*, 625–637. [[CrossRef](#)]
40. Soulsby, R. Chapter 9: Bedload transport. In *Dynamics of Marine Sands*; Ice Publishing: Leeds, UK, 1997; pp. 155–170.
41. Meyer-Peter, E.; Müller, R. Formulas for bed-load transport. In Proceedings of the 2nd Meeting of the International Association for Hydraulic Structures Research, Delft, The Netherlands, 7 June 1948; pp. 39–64.
42. Daneshfaraz, R.; Ghaderi, A.; Sattariyan, M.; Alinejad, B.; Asl, M.M.; Di Francesco, S. Investigation of Local Scouring around Hydrodynamic and Circular Pile Groups under the Influence of River Material Harvesting Pits. *Water* **2021**, *13*, 2192. [[CrossRef](#)]
43. Kim, H.S.; Roh, M.; Nabi, M. Computational Modeling of Flow and Scour around Two Cylinders in Staggered Array. *Water* **2017**, *9*, 654. [[CrossRef](#)]
44. Wang, F.; Zhang, B.; Qi, J. 3D numerical investigation of bridge pier-scour development using a dynamic-mesh updating technique. *South North Water Transf. Water Sci. Technol.* **2017**, *15*, 132–137. [[CrossRef](#)]
45. Wang, S.H.; Yang, S.Y.; He, Z.G.; Li, L.; Xia, Y.Z. Effect of Inclination Angles on the Local Scour around a Submerged Cylinder. *Water* **2020**, *12*, 2687. [[CrossRef](#)]
46. Li, J.Z.; Kong, X.; Yang, Y.L.; Deng, L.; Xiong, W. CFD investigations of tsunami-induced scour around bridge piers. *Ocean Eng.* **2022**, *244*, 16. [[CrossRef](#)]
47. Li, A.; Zhang, G.; Chandara, M.; Zhou, S. Influence of sediment transport rate formula on numerical simulation of local scour around a bridge pier. *J. Sediment Res.* **2022**, *47*, 15–22. [[CrossRef](#)]
48. Sheppard, D.M.; Odeh, M.; Glasser, T. Large scale clear-water local pier scour experiments. *J. Hydraul. Eng.* **2004**, *130*, 957–963. [[CrossRef](#)]

Disclaimer/Publisher's Note: The statements, opinions and data contained in all publications are solely those of the individual author(s) and contributor(s) and not of MDPI and/or the editor(s). MDPI and/or the editor(s) disclaim responsibility for any injury to people or property resulting from any ideas, methods, instructions or products referred to in the content.